Capabilities and Limitations of High Spatial Resolution A.E.S.

Jacques Cazaux, LASSI DTI

Faculté des Sciences BP 1039 F 51687 Reims Cedex 2 France

(Received: Jan. 31, 1997 Accepted: Feb. 20, 1997)

Abstract

Since its early applications for surface compositional analysis, in the late sixties, the capabilities of Auger Electron Spectroscopy (AES) have been pushed in three directions : the improvement of quantification, the conquest of the third dimension and the decrease of the incident probe diameter. The recent development of probes in the ten nm range associated to the intrinsic surface sensitivity of AES make possible its use for the analytical characterization of nanostructures even when they are buried. But new difficulties appear when AES is pushed towards its limits and new strategies are required. The present state of the art of AES from the high spatial resolution point of view is the main subject of this review paper. It begins with the performance of conventional AES to illustrate the spectacular evolution of this technique but also to explain why new strategies are often required and new limitations appear. Selected examples of applications will be given. Finally a new concept, the effective spatial ionization function, for the characterization of small details is also suggested for the first time.

1. Introduction

Auger-electron spectroscopy (AES) is one of the most widely used techniques for surface compositional analysis as well from the basic point of view of surface science as from the technological point of view of industrial applications.

The surface sensitivity of AES results from the short escape depth of Auger electrons (in the 0.3-3 nm range) and these Auger electrons are most commonly produced by bombarding the specimen surface with a 5-25 keV electron beam. One application of AES involves its use for probing the electronic structure of surface but, by far the largest use of AES is in the measurement of the near surface composition of solids. Since the early development of this technique, in the late sixties, the incident probe diameter has also been decreased from the millimeter range down to the ten nm range or below for some specific instruments. Auger spectras can be acquired as the incident beam is rastered across the surface in order to obtain micro analytical images in Scanning Auger Microscopy (SAM). Specimen material can also be removed by concurrent ion bombardment, and it is thus possible to determine the composition of the exposed surface and thus composition versus depth from the starting surface.

In the field of surface analysis with Auger electrons, the present state of the art and the trends are related to the improvements of quantification (i) of depth profiling (ii) of lateral resolution (iii) and all these developments can be applied to the context of characterization of nanostructures. Conventional AES (operated at a lateral resolution in the micron range) can be used if the structure of interest has its nanometer dimension along one direction (the z direction) and is set on a surface : a thin coating for instance. Its composition can be next determinated by using the recent developments of quantitative AES. For buried nanometer thick structures or multilayers systems, in-depth profiling AES has to be applied. Finally 3d nanostructures may be characterized by using the capabilities of high spatial resolution AES (combined to sputter etching if necessary).

But unfortunately, and like for any other microbeam technique, these are intrinsic limitations and the goals i) to iii) are often conflicting to each others. A good quantification process requires, first, to deal with a good spectrum with a high signal-to-noise ratio while a high lateral resolution is achieved with a smaller (and less intense) incident beam and a shorter time for the acquisition of a point spectrum, this in order to obtain, finally characteristic images in a reasonable time. Consequently the quantification of these characteristic images will be, obviously, less accurate than a point quantification.

This review article is mainly concerned with the performance and limitations of high spatial resolution AES applied to the investigation of nanostructures. The basic mechanisms and common principles which applies to all forms

of Auger Electron Spectroscopy will be first given (section 2).
This is followed by a short description of in depth profiling. The capabilities of high spatial resolution AES for the characterization of 3 d nanostructures will be also discussed and illustrated in section 3. The need to decrease the incident spot diameter requires the building of prototypes or the operation of sophisticated instruments (recently available on the market) and the dramatic decrease of the analyzed volume implies the use of new procedures for the image acquisitions. The processing of the whole data set is then facilitated with the help of high performance computers and modern methods such as Principal Components Analysis or Correlation Diagrams. The main limitations of SAM will be also considered ; they concern the investigation of insulating (and radiation sensitive) specimens and of surfaces having large topographic effects.
A new concept for the characterization of small details is also suggested (in the appendix).

2. Basic Principles of A.E.S.

The aim of the present section is just to give a short overview of conventional AES for outlining its common points and differences with high spatial resolution AES (section 3).

2.1 Historical Aspect

In a series of papers beginning in 1923, P. Auger observed and interpreted the effect that now bears his name [1]. An atomic inner-shell vacancy produced by incident X-rays (or electrons, or ions) can de-excite by a two electron process in which one electron fills the inner shell vacancy and the other is emitted from the atom with a characteristic kinetic energy. The possible use of Auger electron emission from solids for surface analysis was suggested by Lander [2] but the early developments of AES started in conjunction with low energy electron diffraction (LEED) when LEED was operated in metal UHV systems marketed commercially [3]. Commercial instruments designed specifically for AES became available in the late 1960's and 1969 has been identified as the effective take-off year for AES [4][5]. Presently AES is a well established technique for surface analysis and for the past ten years, the average number of journal articles that contain reports of AES measurements is certainly larger than 600 per year [5]. Also the principles and applications of AES takes, of course, a large part in any book dedicated to electron spectroscopy or to surface analysis [see ref. 6-8 for instance]. The interested readers are also referred to some special issues of Journals dedicated to the memory of P. Auger when he passed away, at the end of 1993 [9-10].

2.2 Atomic Mechanisms and Surface Sensitivity of AES.

The left hand side of fig. 1 illustrates the excitation process involved in e^- AES (e^- : electron induced) where an incident electron causes ejection of the inner shell (K) electron of atom A (binding energy : $E(A_K)$).
Such an ionization process followed by two de-excitation processes (see right hand side of fig.1) : X-ray photon and Auger electron emissions but the Auger emission probability, a_{ijk}, is greater than the fluorescence yield, ω_{ij}, when the initial binding energy is $E(A) < 10$ keV (see middle part of fig.1). AES is based on the measurement, in the 50 - 2500 eV range, of the kinetic energy of the emitted Auger electrons :

$$E(A_{KLL}) \approx E(A_K) - E(A_L) - E(AL) \qquad (1)$$

Then from the tabulated values [11] of all the Auger lines position, except H and He, the elemental identification for the specimen composition is possible in a way similar to EPMA (Electron Probe MicroAnalysis) where the characteristic photon energies are detected for such an identification.
The similarities between AES and EPMA may also be seen on Fig. 2 where the extension of the ionization zone of AES and EPMA is shown. This zone, in the real space, is obviously the same for the same primary beam energy, specimen and $E(A_K)$ level [12][13]. The principal difference between EPMA and SAM results from the fact that the main X-ray information emerges from the excitation volume. In contrast the only Auger electrons that can be detected with their initial characteristic energy are issued from a surface layer of thickness related to their short inelastic mean frees path (IMPF). The short values of the IMPF of 50-2500 eV electrons in solids in then responsible for the surface sensitivity of AES (and also X-ray Photoelectron Spectroscopy XPS). Fig. 3 shows IMPF values calculated by Tanuma, Powell and Penn for a group of 27 elements (left) and for 14 organic compounds

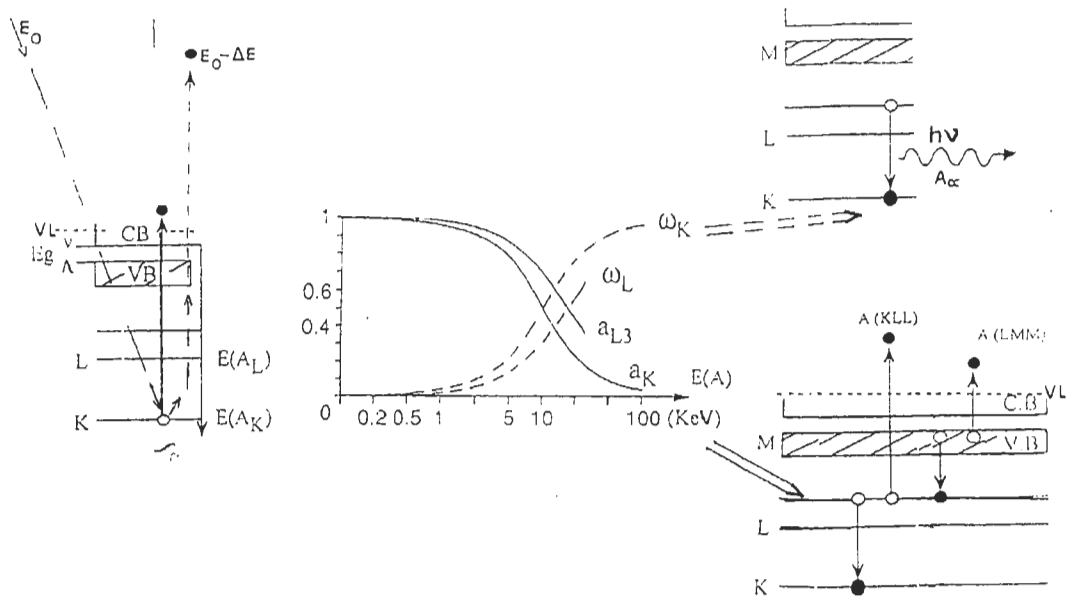

Fig. 1 Basic mechanisms involved in e⁻AES. Left hand side : schematic representation of an inner shell electron excitation with incident electrons Right hand side : schematic representation of the two de-excitation processes in competition ; characteristic photon emission (top) and Auger electron emission (bottom). Their respective probabilities ω_{ij} (or ω_k, ω_L) and a_{ijk} (or a_K, a_{L3}) as a function of the initial binding energy $E(A_K)$ is shown on the middle. The symbols used for the assignment of the Auger transitions are also indicated on the right hand side : A(KLL) transition and A(LMM) or (CVV) transition.

(right) [14]. This plot, as a function of electron kinetic energy, shows that the maximum surface sensitivity occurs in the 100 eV range but it also shows that the IMFP depends on the specimen composition (which is in principle unknown).

Another matrix factor is the Auger backscattering factor, R, which describes the reinforcements, by the backscattered electrons, of the surface ionizations directly produced by the incident electron beam I_o. This factor is normalized to the primary beam contribution so that 1 + R also represents the value at the surface, $\phi(0)$, of the in depth ionization function used in EPMA (see fig. 2). Inspired from a compilation of various calculations and experiments [15], Fig. 4 shows the change of 1 + R as a function of the reduced energy $U(= E_o/E(A_K))$ for different substrates (see also ref. [16] for the most widely used analytical expression).

2.3 Instruments, Spectras and Signal Intensity Measurements

From the instrumental point of view, the main components of an AES apparatus are : an electron gun, a specimen and an electron analyser, all components being set in a ultra high vacuum (UHV) chamber. In opposition to

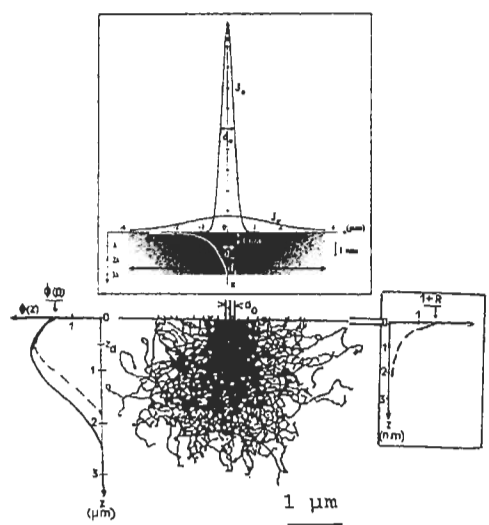

Fig. 2 Pictoral view of the random walk of a 20 keV electron beam into a Al_2O_3 sample (Courtesy O.Jbara). On the left, the in-depth ionization function $\Phi(z)$ is shown for Al(K) ionizations (full line). The dashed lines represent this function when weighted by the attenuation function of emitted (AlKα) X-rays (left) or of emitted Al(KLL) Auger electrons (right). Note the change of the vertical scale between the two. On the top, approximate sketch of the radial distribution function at the surface : j(0,r). It is the sum of the incident beam contribution (relative weight 1) and of the backscattered contribution (relative weight R). d_o is the incident beam diameter.

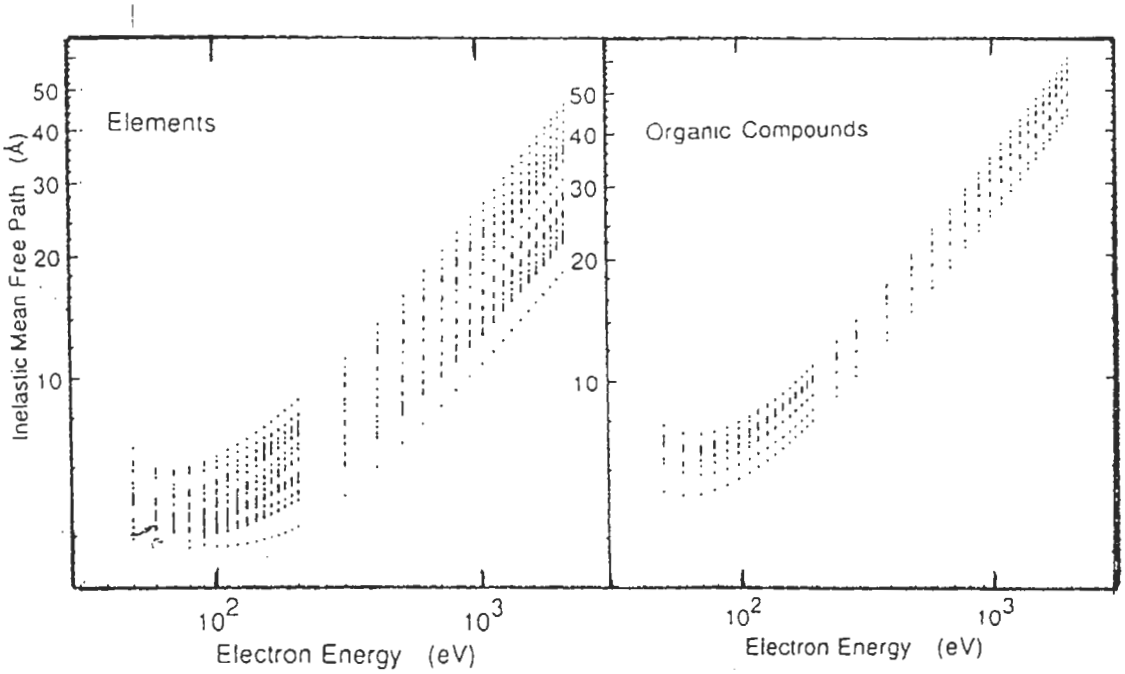

Fig. 3 I.M.P.F. results for 27 elements (left) and 14 organic compounds as a function of electron kinetic energy (from Tanuma, Powell and Penn [14]).

other microanalytical (EPMA, EELS) or microscopical (TEM, SEM) techniques, where the basic architecture of the corresponding instruments has not significantly changed over

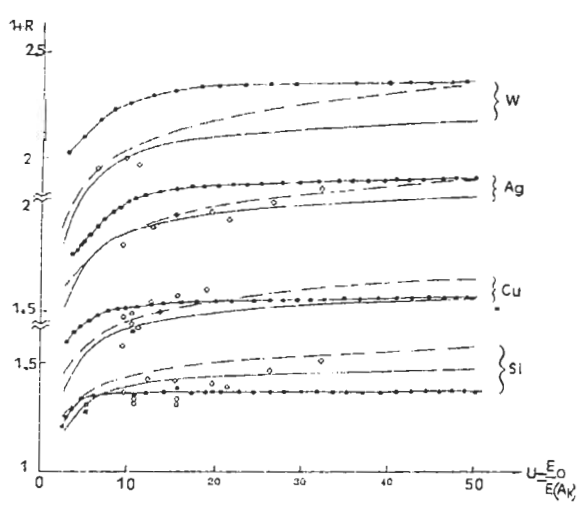

Fig. 4 Change of the factor 1 + R (with R : Auger backscattering factor) as a function of the reduced energy $U = E_o/E(A_K)$ for different substrates : W, Ag, Cu, Si (from top to bottom) and at normal incidence. Compilation of various calculations (including the popular expression of Shimizu [16]) and results (inspired from [15a]).

decades, the architecture of Auger instruments has been deeply modified.

Fig. 5 illustrates (in inserts) the evolution of the marketed instruments from the sixties with also the corresponding change of the incident spot diameter, d_o, and of the primary beam energy, E_o. On the same figure, the d_o and E_o values of two prototypes (one, built at York [17] and the other built at Arizona State University [18-19]) are also shown with in addition that of a STEM instrument equipped with an Auger analyser [20]. It has to be outlined that fig. 5 just indicates the trends of the Auger equipments in terms of approximate periods and approximate incident spot diameter. Also the architectures of the marketed instruments shown here are just indicative and there are different technical solutions for combining a field emission gun (FEG) and an electron analyser of the CMA (Cylindrical Mirror Analyser) type or of the CHA (Concentric Hemispherical Analyser) type [21] or of another type.

At the early developments of AES, the identification of elemental species was made using differentiated spectra acquired in an analog mode with the help of a look-in amplifier, and incident beam intensities in the microamp. range. The acquisition of the first derivative of the electron energy distribution, such as $\partial[EN(E)]/\partial E$ for example, remains very popular because it presents some advantages, among them there is the direct background suppression and the increase of

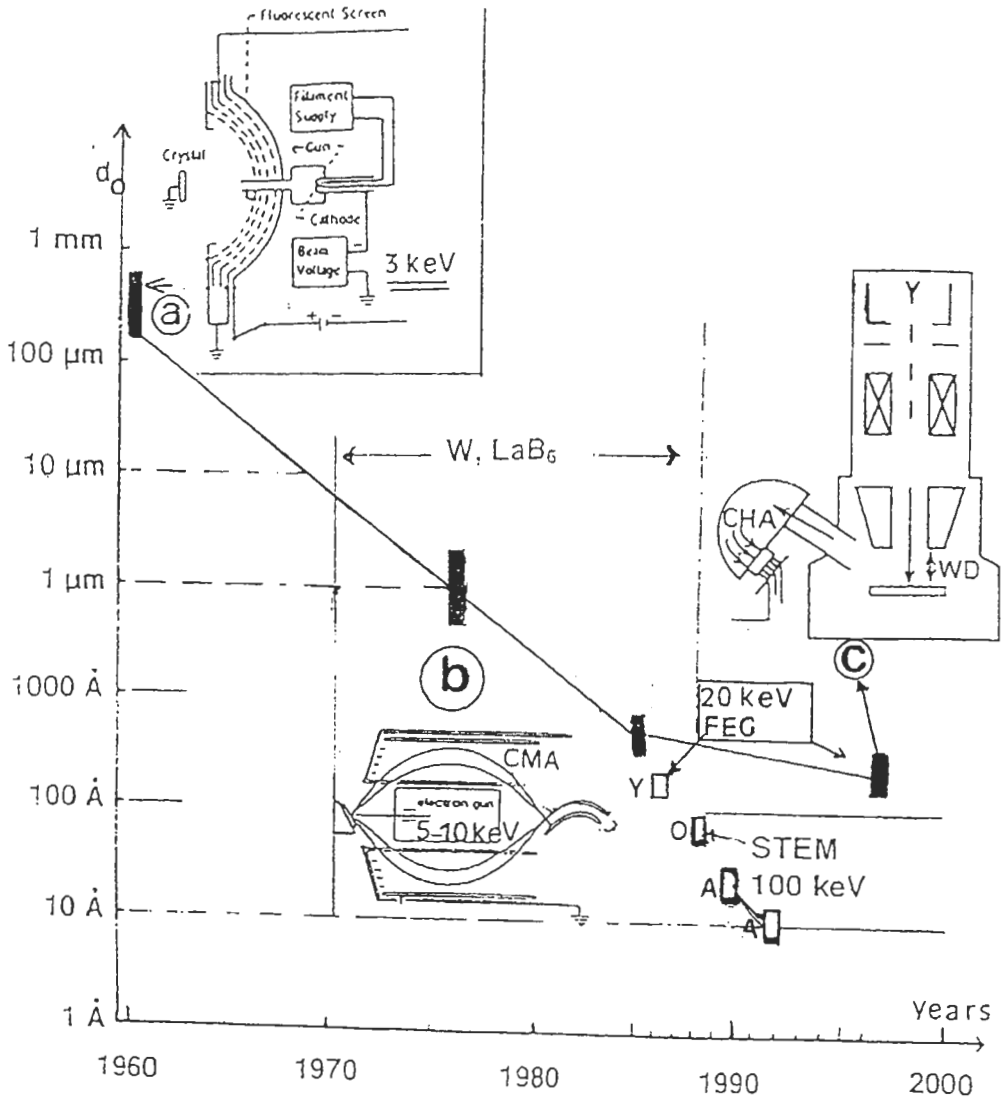

Fig. 5 Trends over the past three decades of the architecture of the marketed instruments, for the incident spot diameter d_o (black rectangles) and for the primary beam energy E_o. Open rectangles show the d_o values obtained with the prototype built at York University (Y) by M. Prutton and co-workers [17], at Arizona State University (A) by J.Venables and co-workers [8-19] with in addition the instrument operated in Orsay (0) [20].
a) The first Auger equipment, in the late sixties, was a LEED instrument with a four grid analyser. Typical values $E_o = 3$ keV . $d_o \approx 1$ mm.
b) In the mid seventies ,most of the analysers were of the CMA type with a thermoelectronic gun either inside (coaxial) or outside the analyser. Typical values $E_o = 5$-10 keV ; $d_o \approx 1$ µm.
c) The last few years the architecture of most of the marketed instruments is based on a UHV (vertical) Scanning Electron Microscope equipped with a Field Emission Gun (FEG) (and often a Schottky emitter). W.D. is the working distance. The typical values are $E_o \approx 20$ keV ; $d_o \cong 10$ - 20 nm.

peak visibility. In addition there is the easier identification of the chemical shifts effect and of the lineshape modification associated to the change of the chemical state of an atom [22][23].
Fig. 6 illustrates this aspect from the derivative spectras of the carbon (CVV) line of some carbides [24] in addition to that of graphite and of diamond [25]. Similar changes have been utilized to identify graphitic or carbidic carbon present on single-crystal catalyst surface at different stages of surface processing [26]. Also in this derivative mode, spectral quantification is simple and easy to make from peak-to-peak

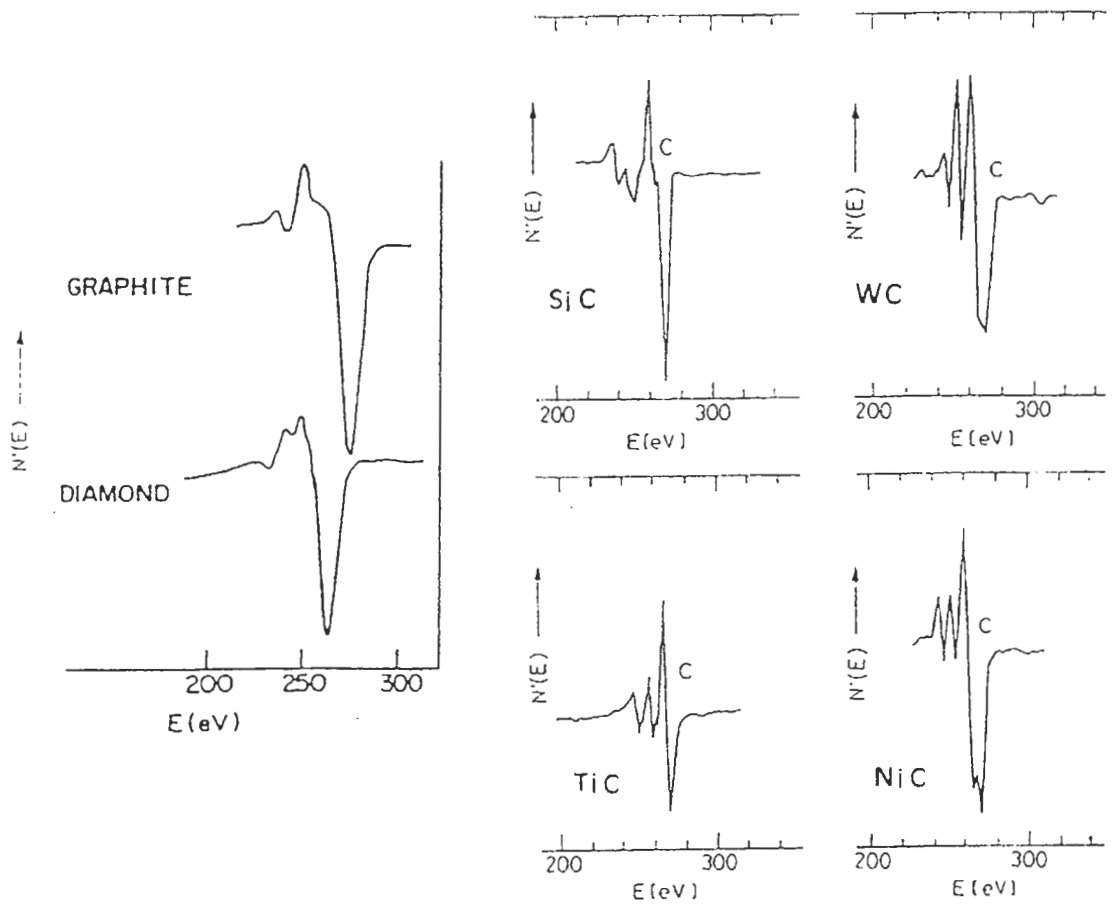

Fig. 6 Changes in both the position and the shape of the carbon (CVV) line for graphite, diamond [25] and for various carbides [24]. The presented spectra are plotted in the form of the derivative of the energy distribution $\partial N(E)/\partial E$ versus electron kinetic energy.

height measurements but to be effective this procedure has only to be restricted to metallic mixtures where there are no spectral peak shape changes and for spectras recorded on one instrument [23]. Many of these problems disappear if the spectra are recorded in the direct spectral mode, N(E) or EN(E), for instance. These direct spectras are always acquired in a digital form by using a pulse counting technique when the incident beam intensity is in the nanoamp. range. In the direct mode a characteristic Auger intensity I(A) is directly related to the area of its corresponding peak obtained after removing a well defined background. The main part of the background results from the tail of the secondary electrons, $\partial\delta(E)/\partial E$, and from the spectral distribution of the backscattered electrons, $\partial\eta(E)/\partial E$. If the whole spectrum is plotted on log-log axes the essential of this background can be removed [27]. The remaining part results from inelastic interactions experienced by the emitted Auger electrons. It appears in the low kinetic energy tails and it is suppressed by linear or integral background subtraction methods [23] or better by the deconvolution method initiated by Tougaard [28].

Fig. 7 gives an example of a direct spectrum obtained in a counting mode [29]. It also illustrates the background removal in quantitative AES and it anticipates on the background subtraction problem in SAM.

2.4 Intensity / Concentration Relationship , Sensitivity.

In conventional AES where only the change of the components' concentration as a function of depth is considered, the detected Auger signal intensity of element A, I(A) is related to its atomic concentration, $C_A(z)$, by :

$$I(A) = I_o \cos ec\ \alpha \int_0^{\infty} [N^{\circ} C_A(z)(1 + R_{A/S}) Q_A dz] a_{ijk}\ e^{-z/\lambda \sin\theta} T_A \qquad (2)$$

where I_o is the incident intensity and α is the

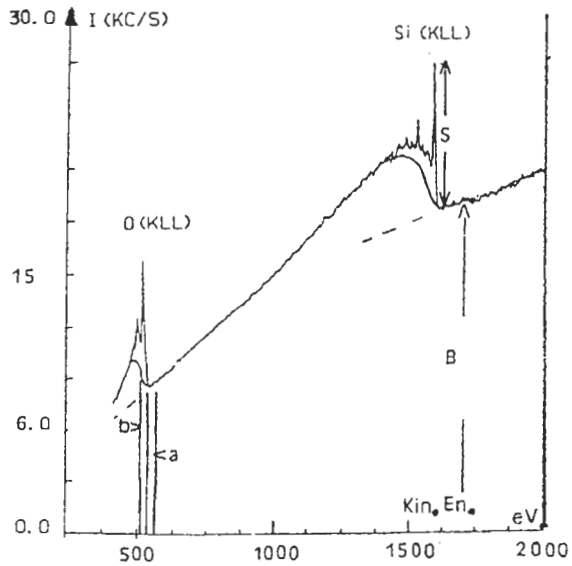

Fig. 7 Experimental EN(E) spectrum obtained in the counting mode on SiO_2 on Si at E_o = 100 keV [from Ref. 29]. Dashed lines correspond to a linear extrapolation of the background (here due mainly to the spectral distribution of the backscattered electrons). Full lines suggest the final result obtained after appropriate methods for background ,B, removal. In SAM elemental mapping only two energy windows are often used (see O(KLL) line) : one, a, after the peak for B ; the other, b, on the peak for S + B. Note the good signal-to-background ratio (~ 1 for this line) obtained at a rather unusual primary beam energy for AES.

angle of incidence. The expression between brackets corresponds to the number of ionized atoms (electronic level i) per incident electron, where Q_A is the ionization cross-section ; $R_{A/S}$ is the Auger backscattering coefficient, R, and the subscript A/S represents the reinforcement of the Auger signal of surface element A by the electrons backscattered by the substrate S ; N° is the atomic density (~ 5.10^{22} atoms/cm^3). Further, T_A is the collection efficiency of the analyser ; a_{ijk} is the Auger yield and the exponential term describes the attenuation of Auger electrons generated in the specimen at depth z when going towards the analyser (λ = attenuation length and θ = take off angle). The attenuation length, λ, is a functional parameter related to the inelastic mean free path (Fig. 3) and to the elastic mean free path of Auger electrons escaping into the vacuum [30-35]. When $C_A(z)$ is a constant over a depth of say, 3λ, the integration leads to :

$$I(A) = I_o N° C_A (1+R_{A/S}) Q_A \lambda \sin\theta \, a_{ijk} T_A \quad (3)$$

where now the normal incidence is only considered for the sake of the simplicity. The surface sensitivity of AES is increased when sin θ is decreased but only 63 % of the signal come from the thickness $\lambda \sin\theta$ and the information depth is usually chosen to be $3\lambda \sin\theta$. This information depth is in the 1-5 nm range depending upon the kinetic energy of the Auger electrons of interest (and upon the take off angle θ).

For a pure element one may write [36] :

$$I^{\infty}(A) = I_o . \beta(A) . T_A \quad (4)$$

where $\beta(A)$ is the quantum yield and is in the 10^{-4} - 10^{-5} range (with $Q_A \approx 2.10^{-20}$ - $2\ 10^{-21}$ cm^2 ; $\lambda \sin\theta \approx 1$nm, $a_{ijk} \approx 1$; N° $\approx 5.10^{22}$ cm^{-3}). In pulse counting, the minimum detectable concentration x_m (in at/at) corresponds to [36] :

$$x_m \approx \frac{3\sqrt{B.\tau}}{I^{\infty}(A)\tau} \quad (5)$$

where B is the background intensity and τ is the channel dwell time for the signal and for the background. x_m is directly related to the S/N ratio [37] by $x_m = 3/(S/N)$ and for the major species it may vary from 10^{-1} to 10^{-4} as a function of the incident beam intensity I_o and of time of acquisition of the spectrum [37]. The medium values (10^{-2} - 10^{-3}) are obtained for $I^{\infty}(A)\tau \approx 10^{\circ}$ counts (and $B\tau$ of the same order of magnitude). These medium values correspond to the usual sensitivity of AES : a fraction of monolayer.

The acquisition of a good spectrum (high S/N) is first required for a good quantitative analysis. Since the earliest applications of AES, considerable efforts have been (and are) devoted to improve its quantification that is to say to deduce the concentrations of the elemental components of a surface C_A, C_B, ... C_N from the measurements of the corresponding intensities, I_A, I_B, ... I_N [22,23]. The accuracy of this deduction was initially rather poor and to improve on this, an international cooperation program has been established (VAMAS Program Technical Working area 2, Surface Analysis) [38]. There are various alternative routes to quantification but all are derived from the use of eq.(2). The difficulties are known [22, 23, 37,38] and some of them have been recently overcome as it can be seen in recent papers related to absolute high resolution digital Auger electron reference databases [39].

In fact one of the main other difficulties is related to the restrictive conditions where eq.(2) applies (in addition to a correct background subtraction for a correct measurement of the Auger intensity, I(A), on the left hand side of eq (2)). The use of eq. 2 implies that the analysed surface is smooth at nearly the atomic scale and that the specimen is amorphous in the corresponding region. This last constraint forbids, in principle the accurate quantification of crystals. Auger electron diffraction permits the direct imaging of surface and interface structures [40-44], but the channelling effects are a serious impediment to quantitative Auger analysis [45, 46].

2.5 Other Possibilities and Limitations of Conventional AES.

AES can also be used for probing the electronic structure of a surface. For this goal the transitions of interest are mainly of the CVV type (ionization of a core level followed by an Auger decay involving two electrons from the valence band : see the A(LMM) transition on the extreme right hand side of fig.1). A detailed theory of the Auger lineshapes was initially developed by Cini [47] and by Sawatzki [48]. This theory has proven extremely useful for analysing Auger - electron lineshape and for deducing information on electronic structure of various systems [49-51]. In this area, the present state of the art can be found in the 120 references, of a recent review paper [52] or in the 36 references of papers only dedicated to the Cu(LVV) lineshape of high temperature superconductors [53] or in the proceedings of the 3rd international workshop on Auger Spectroscopy and Electronic Structures [54].

Independently of any fundamental consideration the combination of the chemical shift effect and the line shape modification can be used for practical purpose in surface analysis. These shifts and modifications can be used as fingerprints for identifying the different chemical states of an atom (see fig. 6) but they are also a major source of systematic error in quantitative AES mainly when peak-to-peak heights acquired in the derivative mode are used for finding the corresponding concentrations [5].

Finally the major limitation of AES occurs when, under fixed experimental conditions, the successive spectras are continuously shifted in energy and distorted in intensity. These effects are related to specimen charging and specimen damage and they may happen simultaneously in the investigation of insulating materials (see ref [55] for an example). Charging effects which may lead to loss of the spectrum have been often observed [56-58] and they may be interpreted as a competition between the secondary electron emission and various electrostatics, electrodynamics phenomenae [59, 60]. At the microscopic scale, the roles of surrounding atmosphere for the possible neutralization of the surface charges [61] of the contamination islands and of structural defects for the charge trapping are not fully understood or are a subject for debate [60]. The internal electric field build up may also lead to the change in composition during AES analysis. This change has been observed in the investigation of glasses where this electric field drives the migration of the mobile ions towards the interfaces [62-64].

In the absence of mobile ions, thin dielectric layers can be investigated by AES and with a reduced shift in energy when there are backed by a conducting substrate (an oxide layer on its metal, for instance). The reason is that the voltage drop between the oxide/metal interface and the vacuum/oxide interface will be very low even if the electric field is very high [60]. This explanation is consistent with the successful experiments, recently reported by Lorang et al [66] on thin oxide films (as standards for an AES data bank).

The electron beam induced damage as observed in AES (or in SEM) has also been widely reported [37,66-70]. The effect of electron-stimulated desorption (ESD) in compounds sets an upper limit to the allowed dose of electrons per unit area [37], and then the incident probe diameter is also limited [36]. It is fun to point out that a possible microscopic mechanism for explaining the ESD effect is the Auger decay which, then, would limit the performance of Auger spectroscopy [70]. For instance the Auger decay leaves two holes in the valence band of alkali halides (see the extreme right part of fig. 1) which transforms the halogen anion into a cation changing then the sign of its Madelung energy. This ion is pushed out of its site because the lack of conduction electrons prevents the initial charge of this ion to be quickly restored.

3. Spatially Resolved AES

3.1 General Considerations

For any kind of microanalytical technique, the

basic strategy for investigating a detail consists in optimizing the signal issued from the detail of interest with respect to the signals issued from its surroundings. AES is basically a surface sensitive technique so that for investigating buried details (situated below the information depth of this technique) there is the need to remove the overlayers of the specimen to allow the details to become surface details. When the detail of interest is set on a surface and when its lateral dimensions are decreased, the same basic strategy consists, in SAM, in focusing the incident electron beam into smaller and smaller probe sizes. In many cases, the use of fine probes is also interesting for acquiring Auger line scan profiles and Auger maps of the regions of interest. (The regions or details of interest being first localized from the use of the instrument in the SEM mode). Of course such possibilities are paid by a less sensitivity (because of the poorer S/N ratio) and, with respect to conventional AES, new constraints appear and new strategies have to be applied. The goal of the present section is to describe the present state of art of spatially (in 3d) resolved AES with a special attention devoted to SAM. Characteristic Auger images may also be obtained in Low Energy Electron Microscopy (LEEM) and the interested readers are referred to the Prof. Bauer's contribution to this meeting and to the references [71,72].

3.2 z-profiling in AES

In AES, non destructive z-profiling is, in principle, possible (down to thicknesses $t \approx 3\lambda$) by variation of the electron emission angle θ. From eq.2, it has been observed that the measured intensity $I(\theta)$ is the Laplace transform of the concentration C(z) [73]. This concentration profile can be, then deduced from the use of the inverse Laplace transform of the measured angular intensities.

This procedure is widely used in XPS [74-78] despite the amplification of the measurement errors in the solution of the inverse problem [23, 37, 73]. If a precise C(z) profile is difficult to obtain, the variation of the take-off angle θ in XPS permits, at least, to distinguish between a thin overlayer of an element A on a substrate B and an homogeneous surface of composition $A_X B_Y$. It also permits to estimate the overlayer thickness t from the simple tilt of the specimen [23,74].

With standard spectrometers similar experiments are far less easy in AES because the tilt of the specimen also changes the backscattering factor R and the cosec α values of eq.(2). At fixed incidence angles, polar angle resolving experiments with parallel detection remains possible but they require the electron analyser to be adapted [44,79]. Consequently from only one Auger spectrum, the "a priori" knowledge of the specimen stratification is often needed for the determination of either the thickness or the composition of the overlayer.

To go deeper than 3 λ in the in-depth distribution analysis, the need is to use a destructive technique either outside (ball cratering, chemical bevelling) or better inside the Auger instrument. There are very few investigations carried out by AES that do not involve sputter etching either to remove surface contamination or in the production of the called Auger depth profile. Auger depth profile is a combination of surface analysis and sputtering. It has opened the third dimension to AES and the conquest of this third dimension is one of the most (if not the most?) significant developments of AES for the past few years. Besides the ion beam bevel section developped in conjuction with finely focused incident electron probes (see 3.4), the recent progress in Auger depth profile (developped in conjuction with standard incident electron probes) results from technical developments related to 'in situ" ion etching at oblique incidence with or without Zalar rotation system [80,81]. It also results from a careful analysis of the physical parameters involved in the sputter mechanism and the emission of Auger electrons [82-84]. The third development of Auger depth profile is related to the full exploitation of the collected data using factor analysis (FA) [22, 85-87].

In such a situation where successive spectras are acquired, this very powerful mathematical method is able to indicate the number of components (or factors) which are varying within the data set and to classify them as a function of their relative weight (down to the extra factors entirely related to noise). The shift in position and the change in the lineshapes associated to changes in the chemical environment (as seen on fig.6) can be fully exploited by using FA in order to obtain, finally, depth profiles of the elements with respect to their chemical bonding states. Factor analysis is also useful in interpreting Auger spectras where peak overlap problems occur ; it

also applies to any time series of Auger spectras such as that obtained, at fixed probe, during oxygen exposure (oxidation studies) or during nucleation and growth processes or that obtained during an Auger line scan on a surface. The association of Auger depth profiling and FA is widely used for the investigation of magnetic/non magnetic superlattice structures [83] (see also [88-90] for some other recent applications and fig. 8a for an illustration [91]). However excellent the use of FA is for the analysis of AES lineshapes, there is the requirement of standard spectra and the problem of deciding whether or not a factor of minor statistical importance should or should not be considered. For overcoming these difficulties, the use of neural pattern recognition has been recently suggested as an alternative route for post-processing AES spectra [92].

Independently from the data processing, three physical parameters influence the depth resolution from Auger putter depth profiles. These parameters are : atomic mixing, surface roughness and information depth [83]. The relative influence of each of them has been reported for Ni/Cr multilayers [93][94]. Fig. 8b illustrates the fact that sharpness of different / interfaces can reach the nm range for Fe/Cr multilayer structures grown by MBE on a (001) GaAs surfaces [95].

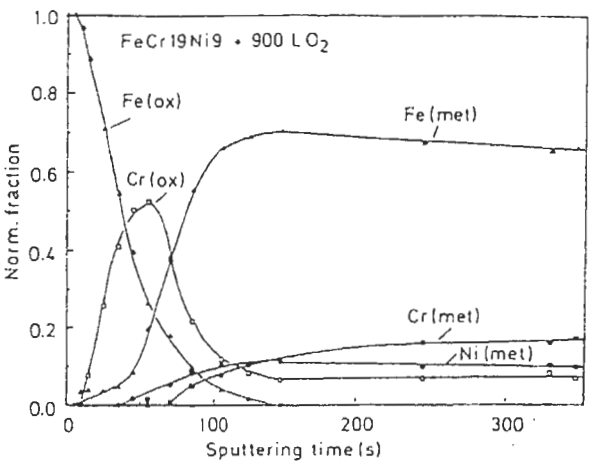

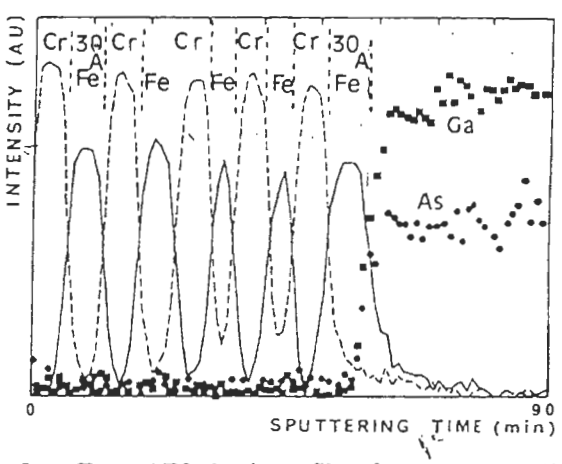

Fig. 8 Top : AES depth profile of an Fe Cr 19 Ni 9 alloy after oxidation. The use of FA reveals six components and least square fitting yields the quantitative fraction of each identified component. Sputtering rate for Ta_2O_5 : Z= 0.3 Å/s. Inspired from [13] and [91].
Bottom : A.E.S. depth profile of five Fe (30 Å)/Cr (30 Å) bilayer structure grown on a GaAs substrate. inspired from [95].

3.3 Incident Probe Diameter and Lateral Resolution

In the past, a large number of papers have been devoted to the lateral resolution problem of SAM. It was particularly important to see whether the spatial resolution limits are determined by the incident electron beam diameter d_o (see fig.2) or by the lateral extent of the backscattered contribution, R [96 and ref. there in]. In the first case, there are some advantages to increase the primary beam energy E_o (see below). In the second case, there is the need to decrease E_o (down to 3 keV, for instance) for suppressing the backscattered contribution (see on fig.4 the evolution of R at low U, or E_o, values).

In optics, the lateral resolution, ℓ.r., characterizes an instrument and is defined as the minimum distance between two points for which the two points are resolved. This resolution can be deduced from the point spread function (PSF) of the instrument (or from its Fourier transform : the transfer function) using next either the Rayleigh criterion or the Sparrow criterion [96]. The PSF function, or more precisely, the line spread function (LSF) may be deduced from the first derivative of an experimental profile taken across an abrupt interface ; such a profile corresponds to the edge spread function (ESF). When applied to SAM, this definition leads to the fact the lateral resolution is only related to the incident spot diameter alone (ℓ.r $\approx$ d_o) even when the Auger backscattering factor, R, is close to the unity and the suggested procedure to measure it, the full-width at half maximum of the L.S.F., is better than the arbitrary criteria often applied to the

experimental ESF : the distance between points giving 10 % and 90 % (or 20 % and 80 % or 25 % and 75 %) of the maximum Auger signal. This definition and this experimental procedure can be easily transposed to depth resolution of Auger depth profiles. In SAM, the advantage of this definition is that the obtained lateral resolution is not specimen (or matrix) dependent. The lateral resolution ℓ.r differs from the minimum dimension, d_m, for a detail to be detectable (or the elements composing it to be identifiable) which obviously depends, via the signal-to-noise ratio of eq.5, of the incident beam dose and of the elements composing the specimen : then d_m can be either larger or smaller than ℓ.r (or d_o) [96].

The lateral resolution also differs from the minimum dimension, d_q, for a detail to be quantifiable. As shown on fig. 2 (top insert), the radial distribution of the emitted Auger electrons may extend over few tenths of microns or more depending upon the value of the primary beam energy, Eo and of the substrate composition. Consequently the application of quantification methods of conventional AES to quantification in SAM requires to consider that the analysed volume is defined by the lateral dimension of the backscattering halo, d_R, (even if a significant fraction of the signal, 1/(1+R), comes from the area $\pi d^2_o/4$) and by a height of $3\lambda\sin\theta$ (even if 66% of the signal comes from the depth $\lambda\sin\theta$). The concentrations then deduced are postulated to be that of elements uniformly distributed inside this (rather large) analysed volume. When high resolution SAM is then performed for analysing a small detail (such a grain boundary), the mean concentration then evaluated may be very different from the reality.

Instead of dealing with an analysed volume having a blurred border, it seems more convenient to use an effective 3 dimensional response function for AES, which takes into account the different probability for an atom to be ionized (as a function of its lateral coordinate) and the probability for the corresponding Auger electron to be detected (as a function of its z co-ordinate).

Such an effective spatial ionization function is discussed in the appendix and it can be derived from the extension to 3d of eq.2 at normal incidence

$$I(A) = \int_0^\infty [j_o(r) + j_R(r)] 2\pi r dr \int_0^\infty N^a \; C_A(r,z) Q(A_i) a_{ijk} \; e^{-z/\lambda \sin s\theta} dz . T_A \qquad (6)$$

where $j_o(r)$ is the radial distribution of the incident beam density. $j_R(r)$ is the effective radial distribution of the backscattered electrons where "effective" means that the angular and energy distributions of these b.s. electrons are normalized to the efficiency of incident electrons for the production of the Auger electrons of interest (i.e. at fixed primary beam energy, E_o, and angle of incidence α).

This leads to :

$$I_o = \int_0^\infty j_o(r) 2\pi r dr \qquad (7)$$

and

$$R_{A/S} I_o = \int_0^\infty j_R(r) 2\pi dr \qquad (7')$$

Eqs (6),(7) and (7') may be used for finding the $C_A(r,z)$ values (see appendix). For such a goal, the radial distribution of the incident beam $j_o(r)$ has to be known like it is in Electron Energy Loss Spectroscopy (EELS) [97]. The effective radial distribution of the backscattered electrons which may be deduced from the use of Monte Carlo simulations [98]. It is also possible to use mathematical models for performing such calculations [96,99].

For example Gaussian distributions may be postulated for $j_o(r)$ and for $j_R(r)$:

$$j_o(r) = \frac{I_o}{\pi \sigma_o^2} \exp -(r^2 / \sigma_o^2) \qquad (8)$$

and

$$j_R(r) = \frac{R_{A/S} I_o}{\pi \sigma_R^2} \exp -(r^2 / \sigma_R^2) \qquad (8')$$

where j_R results from the convolution of the backscattered response to a point excitation (lateral parameter b) by the $j_o(r)$ function [96, 99] : $\sigma_R^2 = \sigma_o^2 + b^2$ (9), for Gaussian radial distributions.

Finally, in the case of dispersed details on homogeneous substrates when at least one component of the detail is not in the substrate (or vice-versa) it is rather simple to obtain the spectrum due to the detail alone from a subtraction of the spectrum acquired on the detail to the spectrum acquired on the substrate (and far from the detail). The quantification of

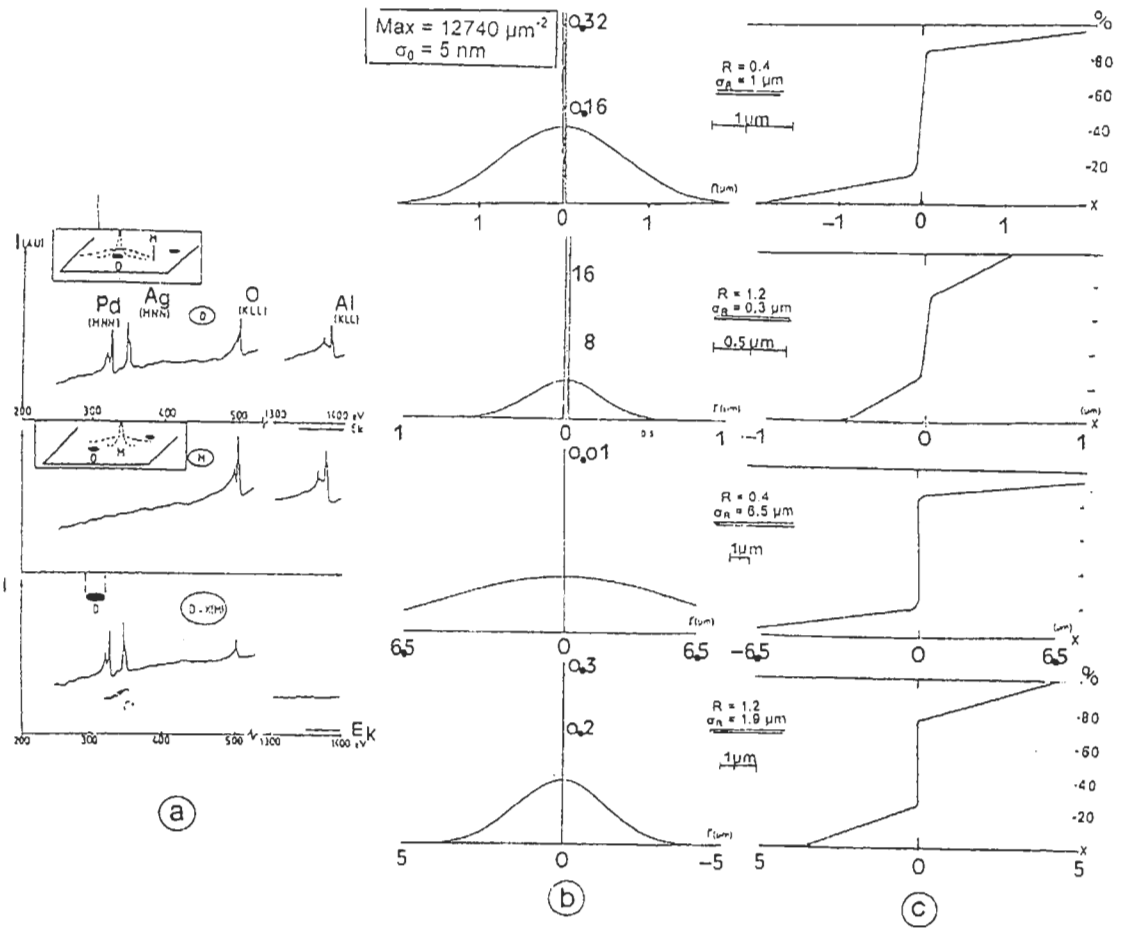

Fig. 9 a) Principles for AES quantitative analysis of a small detail (from [96]) (simulation on Ag Pd grains dispersed on aluminae where, a priori, Al is not expected to be in the detail). The Auger spectrum related to the detail alone (bottom) results from the subtraction of the spectrum obtained on the detail (top) to the spectrum obtained on the matrix (middle). The weighting factor K is adapted to cancel the Al contribution.
b) Point Spread Function deduced from eqs (8) and (8') with (from top to bottom). $R_{A/S} = 0.4$ and $\sigma_R \cong 1\mu m$; $R_{A/S} = 1.2$ and $\sigma_R = 0.3\mu m$; $R_{A/S} = 0.4$ and $\sigma_R = 6.5\ \mu m$: $R_{A/S} = 1.2$ and $\sigma_R = 1.9$ µm. These values nearly corresponds to Al ($R_{A/S} = 0.4$) and W ($R_{A/S} = 1.2$) substrates irradiated by a 20 keV (top : the first two) and a 60 keV (bottom ; the last two) electron beam energy [99]. The incident electron beam parameter remains the same $\sigma_0 \approx 5$ nm (or $d_0 \approx 10$nm). The ratio between the amplitude of the backscattered contribution with respect to the primary one is given (at r = 0) nearly by $R_{A/S}\ \sigma^2_0/\sigma_R^2$ leading to a vertical scale where the maximum of the incident beam density is 12 740 (in μm^{-2} units) for the four diagrams. The respective lateral extent are proportional to σ_R and to σ_0.
c) Corresponding Edge Spread Function.

the detail may be next performed from the use of the sum rule : $\sum_{N}^{A,B,C} C_N = 100\%$.

Fig. 9 (a) illustrates this procedure (from ref [96]) and also some aspects of this subsection concerning the PSF (9b) and the ESF (9c) obtained from the use of eqs.(8) and (8') and related to Al and W substrates at $E_0 = 20$ keV and at $E_0 \approx 60$ keV (see also figs. 5.30 and 5.31 of ref. [23] for other examples). Some other practical aspects and strategies are suggested in subsection 3.6.

3.4 Instrumental Arrangements for SAM.

The principle of SAM was first demonstrated by Mac Donald and Waldrop [100]. An early practical instrument was built by Todd, Poppa and Veneklassen with a miniature field emission gun set inside a CMA and operated at 5 keV [101]. More recently two prototypes have been built in two universities. The different strategies being adopted illustrate very well the conflictual choice between lateral resolution and quantification (as this choice has

been suggested in the above subsection). At York University, the emphasis was placed upon the technique required to quantify images in order to map the variations of the chemical composition in the surface and spatial resolution was a secund priority. Described by Prutton et al [17] this instrument is referred to as MULTI spectral SAM (MULSAM). Two different Field Emission Guns (FEG) can be operated ; their main characteristics are : E_o = 20 keV ; $I_o \approx$ 6nA ; d_o(FWHM) $\approx$ 100 nm ; or are : $E_o \approx$ 1 - 15 keV ; I_o = 10 nA and $d_o \approx$ 20 nm (at 5 keV). This instrument is also characterized by the variety of detectors being operated (see subsection 3.5) and among them, the fifteen detectors set at the exit of the CHA for a parallel detection of the Auger spectras.

At Arizona State University, the emphasis was placed upon the lateral resolution and the instrument is referred to as MIDAS (Microscope for Imaging Diffraction and Analysis of Surfaces) [18, 19, 102, 103]. This instrument is based upon a heavily modified STEM operated at E_o = 100 keV, the incident spot diameter may reach the 1-2 nm range for a nA intensity [18]. The specimen is set in a magnetic immersion lens and a part of the structure of this lens acts as a paralleliser in such a way that almost all the emitted Auger electrons enter the CHA [104, 105], optimizing the collection efficiency of this analyzer (the factor T_A in eq.(2)). A spatial resolution of ~ 3 nm in Auger peak images has been obtained on bulk samples and of 1 nm on thin specimens. Some Ag particles as small as 1-2 nm in diameter and containing as few as 10 Ag atoms have been also detected [19-102]. The advantage of using such an unusual high primary beam energy, results from the increase of brightness of the FE gun and from the decrease of the background (because η does not significally change between 20 and 100 keV and is spread over a larger energy range, then $\partial\eta/\partial E$ decreases). For unsupported thin films, the background is decreased again and the analysed volume is exactly limited to the incident beam irradiated area. This decrease of the background partly compensates the slight decrease of the cross-section Q_{Ai} (E_o) [29] for the sensitivity point of view.

Previously, in Orsay, the same primary beam energy was used in a marketed STEM but equipped with a CHA, in order to perform SAM experiments when the specimen is set outside of the pole pieces [20, 29, 106]. A sub-ten nm resolution was attained with a 8 nm probe size (and 8nA intensity). The elemental analysis of sub-ten nm Pd particles was performed and the number of Pd atoms being detected was estimated to be less than 4 000. A minimum detectable concentration less than 2.10^{-3} was also attained by the detection of a silicon submonolayer buried in a GaAs matrix.

The last generation of SAM instruments that are presently available on the market are based on the architecture of UHV SEM instruments (see fig. 5 : c). They take benefit of Schottky Field emission sources giving a one-nA beam current in a beam diameter in the 10-20 nm range at $E_o \approx$ 15 - 25 keV. Batteries of detectors are operated at the exit of the electron spectrometer for a parallel detection. The conflicting constructional requirements are the formation of an intense fincly focused incident beam and the efficient collection of Auger electrons [107]. On the one hand, the optimum probe is achieved at a point situated in the pole pieces of EM column. On the other hand and except the elegant solution of Kruit and Venables [104], the specimen has to be set in a free field region for preventing the undesirable deflection of the emitted electrons by the fringing fields. Also the use of a significant working distance (W.D) between the end of the EM column and the specimen presents various practical advantages related to the specimen rotation, its ion cleaning as well as the ability to surround it with additional detection systems (ie : b.s electron detector).

A good example of a useful additional attachment is the "ion beam bevel section". This recent development transforms the good lateral resolution of modern SAM instruments in an excellent depth resolution [108]. With this method, a finely focused ion beam is rastered in such a way as to sputter a very shallow bevel into the surface of the sample. Vanishingly small bevel angles are possible leading to magnification of one thousand or more between the vertical (depth) scale, z, and the nearly horizontal x' scale along which an Auger line scan is performed. Fig. 10 illustrates the principle of this technique and it gives also two examples of applications (inspired from the excellent review paper of Skinner dedicated to the role of AES in the semiconductor industry [109]). Other systems of interest for the study of magneto-optic recording media and giant magneto resistance effects have been explored by using this technique in conjunction with the

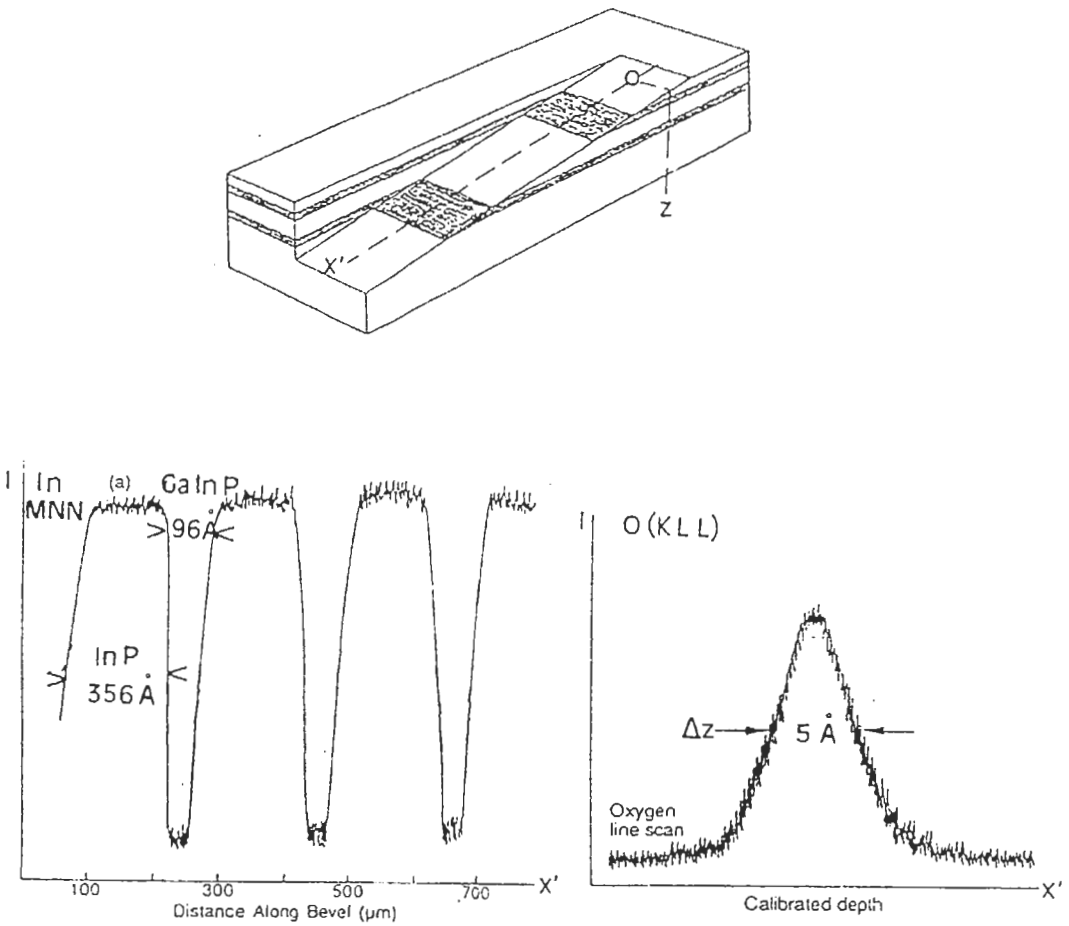

Fig. 10 Top : Principle of the ion beam bevel section : An Auger line scan along the bevel (x' direction) is converted into depth analysis (z direction). The magnification is M = cosec (Oz,Ox'). Bottom (left): Auger In (MNN) line scan across ion bevelled section of GaInAs/InP superlattice (from Skinner [109]). Bottom (right) Ion bevel section of a 5Å oxide at a polysilicon/Si interface : Ox^x profile using the O(KLL) Auger line (from Skinner [109]).

use of Principal Component Analysis and Factor Analysis [110][111]. Computer controlled ion beam bevel sectioning may also be applied to the investigation of more heteregeneous systems where the ion microscalpel is used to remove a part of the materials above the detail or the interface of interest, in order to study next the revealed interface or detail with SAM [112] [113].

3.5 Elemental Mapping in SAM : Problems and Remedies.

This subsection is devoted to the specific problems for elemental mapping in SAM with respect to point analysis in conventional AES (as described in section 2).

3.5.1 Signal Acquisition and Measurements

For incident probe intensities in the 1- 10nA range, from eq.(4), the detected Auger signal intensity is expected to be in the 10^4 c/s range for a pure element (with β (A) $\approx$ few 10^{-4} and T $\approx$ few 10^{-2}). In the sequential mode of acquisition of a (point) spectrum, at least 100 seconds are required for exploring only 100 channels with a dwell time of one second per channel. Then the minimum detectable concentration will only be of around few percents (eq.5) and the total time for the data acquisition of 64 pixels x 64 pixels images will be of around one hundred hours. This total time may be reduced down to one hour if the dwell time per channel is reduced to 10^{-2} s but the expected sensitivity (few ten %) will be very poor.

This simple estimate explains the need of either using a detection of several channels in parallel at the exit of the analyzer [17] or optimizing the collection efficiency, T_A, of the emitted signals [18,104]. In this field a major breakthrough of

SAM will be obtained when the record of the full Auger spectrum will be possible over 1024 independent channels, like it is the case in EELS [114,115]. For slightly different technical reasons, the present situation of SAM is similar to that of SEM EDS (Energy Disperse Spectroscopy) where the acquisition time for elemental mapping with the emitted X-rays is also of the order of the hour. A practical consequence of the present state of the art in SAM is that only two channels per element are used (see fig.7) one for collecting the S + B intensity and the other for collecting the background intensity (on the high energy side of the corresponding peak). The digital mode of acquisition is always used and the chemical shift effect may be exploited only when this shift is rather large such as in Si/SiO_2 or Mg/MgO systems where it is in the 15 - 20 eV range.

The other informations contained in the peak shape (see fig. 6) may be (and are) used in AES point analysis or in AES in depth profiling but they cannot in elemental imaging in SAM. In principle, the characteristic signal intensity I(A) is just deduced from the subtraction of the contents of the two parent channels without any of the sophisticated background subtraction frequently used in conventional AES (see subsect. 2 and ref [28]). The attempt to linearize the background below the peak of interest as it is performed in York [27] is a noticeable exception to the simple subtraction approach.

3.5.2 Backscattering Factor Effects.

The intensity concentration relationship (eq.2) used in SAM requires knowledge of the Auger backscattering factor, $R_{A/S}$, which in turn requires knowledge of the substrate composition when the Shimizu (et al) expression is used directly [16,30]. When SAM is performed this substrate composition may change from place to place influencing then significantly the characteristic Auger signal intensity (see fig. 4). Barkshire et al [116] resolve this problem by detecting simultaneously the electron backscattered current in a scanning Auger microscope. The backscattered electron detector is calibrated (for many elements) and the signal is related to the effective atomic number of the substrate. This is then used to calculate the Auger backscattering factor from the expressions proposed by Shimizu et al at selected angles of incidence ($\alpha = 0°$, 30° and 45°).

Based on the same philosophy (determination of η and then the calculation of R), an alternative approach [117] consists in 1) The determination of η based on the measurement of the specimen current and 2) The calculation of R by using an expression correlating the Auger backscattering factor R and the electron backscattering factor η [15].

This last approach has been also successfully used for the determination of thickness maps of thin coatings by SEM EDS [118]. Each of the two methods may also be applied to Auger in depth profiling where the change of the relative signal intensities is also strongly influenced by the change of substrate composition during the experiments [116].

3.5.3 Topographic Effects

When the incident beam is scanned along a surface, the change of the local slope changes the incident angle α and the take-off angle θ (see top of fig. 11) influencing then the detected intensities (via the influence of α and of θ in eq.2). This type of topographic effect dramatically increases when the incident spot diameter is decreased (bottom of fig. 11). Various approximate corrections have been proposed [17, 119 - 121]. All are based on the fact that, similarly, the background intensity is also influenced by topographic changes. The discussion is often limited to the best weight to give at the measured background intensity (and sometimes to the best kinetic energy where the background has to be measured) for the best topographic correction. Presently it seems that the best approach for correcting rather large topographic effects is the use of signals issued from four backscattered electron detectors [122]. Combined to the ratio of Auger peak height to a background count rate, this use permits the simultaneous correction of topographical and backscattering artefacts [123].

For samples, homogeneous in composition, one may observe (eq.2) that all the characteristic intensities, I(A) I(B)..., are influenced by the same angular factors (cosec α and sin θ). Ratioing these intensities, I(A)/I(B),..., it is easy to cancel these angular effects except those related to the change of $R_{A/S}$ as a function of α [15]. For rather smooth surfaces this change can be considered as a second order effect.

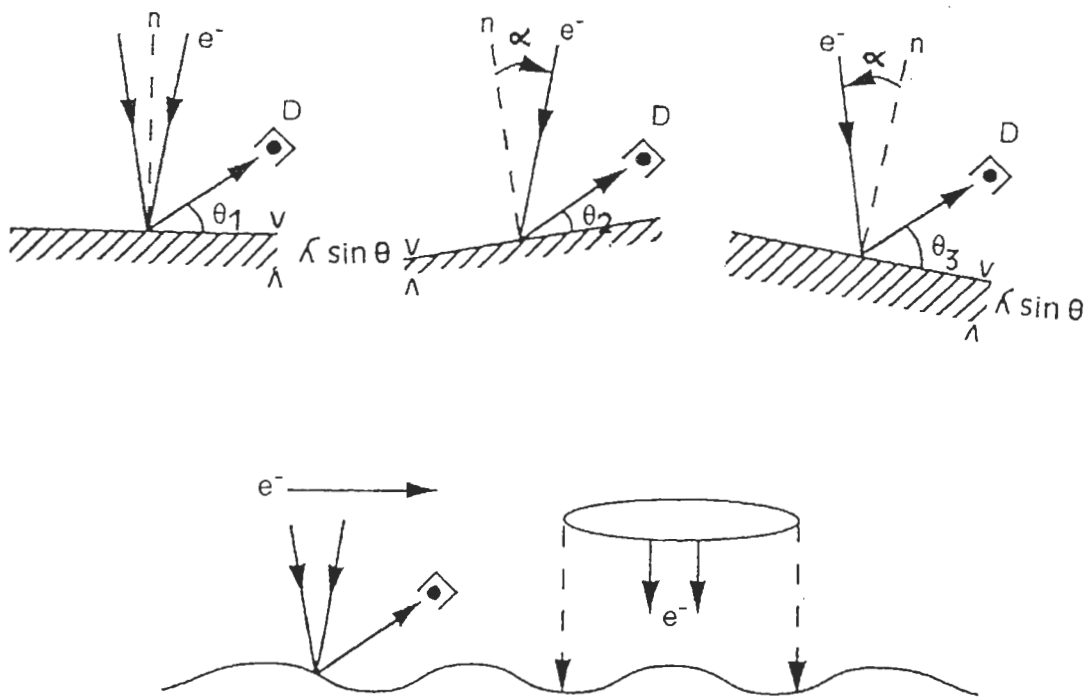

Fig. 11 Top : Topographic effects on a rather smooth surface. The local change of the slope mainly changes α and θ, changing then the intensity collected by the detector, D. Bottom : These effects are more pronounced for fine probes than for a wide illumination (which smoothes these effects).

More difficult to solve is the problem of topographic effects associated to surfaces being heterogeneous in composition and presenting sharp edges or steps or wells. Inspired from the work of El Gomati et al [124], fig. 12 a shows the main effects : the shadowing of the detector by a step (1) and the undesirable extra contributions (2). From the use of M.C. simulations, the physical processes involved in these effects are well understood but conflicting conclusions have been emitted on the best choice of the primary beam energy for minimizing these effects [125-126]. The strategy certainly depends upon the geometry of the instrument and of the investigated surface.

In the semiconductor industry, the topographic effects are sometimes limiting the applications of SAM for the analysis of highly integrated semiconducting devices. As shown on fig. 12 b, the analysis of the bottom of a well with a high aspect ratio, h/w, is not possible when the emitted electrons cannot enter directly into the analyser. The unique solution is to use "ion beam bevel section" to try to remove the curb of the well (?) or to suppress to obstructed pixels in the final image[123c].

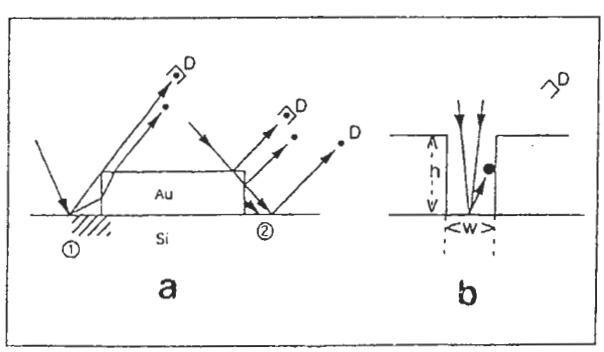

Fig. 12 a) Inspired from El Gomati et al [124], shadowing effects of the detector, D : 1 ; and extra contribution effects : 2 .
b) The signal issued from the bottom of the well cannot directly enter into the detector when the well has a too high aspect ratio, h/w.

3.5.4 Crystalline Effects

Crystalline effects are expected to be more probable in SAM than in conventional AES because the decrease of the incident beam diameter increases its probability to irradiate a single microcrystal while a wide illumination averages the contribution of numerous microcrystals.

3.5.5 Charging Effects and Radiation Damage.

The electric field build up associated to electron irradiation of insulating materials is an increasing function of the density of the charges being trapped in the specimen (see ref. 60 for details). Then scanning the electron beam leads to display these charges along a rather wide surface. Consequently charging effects in SAM are expected to be similar to that observed in conventional AES for similar doses of irradiation. More, the optimization of the scanning frequency may minimize these effects (the charges in excess being evacuated between two successive scans). On the opposite the operation of a finely focused and fixed probe (for a local analysis of a detail) is expected to lead to very large and very spurious charging effects. The electron beam blanking may be a possible solution. Being also approximately dose dependent, radiation damages are expected to have the same dose dependent behaviour [60]. Electron stimulated desorption leads to difficulties for the characterization of some nanostructures with SAM but ESD may be also used to fabricate them [70]. Most of the radiation damage effects are mainly characterized by a change in the surface chemical composition of the irradiated specimens. Oxygen desorption from SiO_2 and Al_2O_3 may lead to the fabrication of metal (or semiconductor)/oxide systems (like Al/Al_2O_3 or Si/SiO_2) by a low energy electron bombardment of the initial bulk oxides. The place where these systems have to be located can be easily selected by the use of the scannable electron beam (of SAM). Similarly one may imagine the fabrication of alkali metal/alkali halides systems from the electron bombardment of halides mainly when the halogen is volatile (F and Cl). Generally the metal coating is expected to be polycrystalline because of the lattice mismatch between the metal and its halide. However a more favourable situation occurs for MX_2 compounds like CaF_2 where the crystal structure of the metal and of the compound is the same, b.c.c., and their respective lattice parameter very close to each other (a = 5.46 Å for CaF_2 and a = 5.57 Å for Ca) [70].

3.5.6 Image Processing

SAM is based on the acquisition from place to place (x_i, y_i) of spectras relating the intensity as a function of the kinetic energy of the detected electrons $I(x_i, y_i) = f(E_K)$. It is a microanalytical microscopy based on similar principles as EELS imaging or SEM-EDS imaging for the point of view of image processing [17b, 115]. Then, the whole data set may be displayed in a space of axis Ox, Oy and E_K in which the contains of a given voxel (dimensions : Δx . Δy . ΔE_K) is the intensity acquired at a point x_i, y_i and at the energy E_{Ki} (for the energy window ΔE_K). The image-spectrum volume may completed by other signals collected when the incident beam is scanned on the surface, such as the backscattered (and the secondary) electron signal η (x_i, y_i) [and $\delta(x_i,y_i)$] for instance (see fig. 13a). All the voxels' informations being in a digital form it is next easy to manipulate this volume in order to extract an Auger point spectrum, or an Auger line profile (PS and LP respect. on fig. 13a). Selecting a given energy E(A) it is also easy to display the image which corresponds to the change of S + B of element A as a function of the x,y co-ordinates. A simple background removal may be obtained from the substraction, pixel per pixel, of the iso-energy images obtained on the peak to that obtained on the background. More sophisticated manipulations may also involve, in addition, other planes such as the η plane, η (x,y) for removing the Auger backscattering effects, for instance.

When the $C_A(x,y)$, $C_B(x,y)$ maps have been obtained or by starting from the initial $I_A(x,y)$, $I_B(x,y)$ images, it is next very useful to deal with correlation (or scatter) diagram technique. Proposed by Browning [127] and widely popularized by Prutton et al for SAM [17b, 128-130] this technique applies for any kind of spectromicroscopy [12]. For a binary alloy, AB, it consists in displaying the characteristic intensities (or concentrations) of each pixel (of an image or a profile) in a I_A vs I_B (or C_A vs C_B) diagram (see fig. 13b). A simple inspection of such a diagram permits to estimate : the number of different phases, A_x B_y, their relative weights, and to detect the existence of artefacts or of deviations from the statistical fluctuations of the number of counts. By windowing one cluster of pixels (related to a specific phase) it is next possible to find where they are located in the direct (x,y) space. This technique may be easily extended to multielement mapping [127] and the scatter diagrams may be displayed in three dimensions [129].

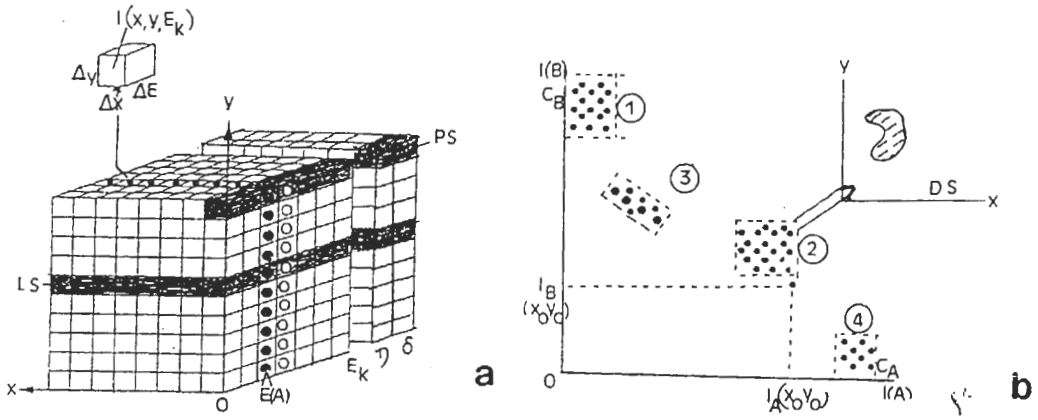

Fig. 13 a) Image spectrum. In the x,y, E_K space, the row PS, in black grey, is a point spectrum and the plane L.S., in black grey, is an Auger line profile parallel to the x-axis. A simple background removal is obtained from a substraction, pixel per pixel, between the image corresponding to a peak at energy E(A)(full symbols) and the image corresponding to the background above the peak (open symbols). Other manipulations may involve the plane $\eta(x,y)$ or the plane δ for Auger backscattering corrections or topographic corrections for instance. The dimensions of each voxel correspond to the lateral resolution (Δx, Δy) and the energy resolution (ΔE).– Inspired prom EELS [115b] but adapted to SAM –

b) Schematic principle of correlation (or scatter) diagram technique. The intensities (or concentrations) obtained for a given pixel (position x_o, y_o in the direct space) fix the position of this pixel in a I_A vs I_B diagram and the operation is repeated for all the pixels of the characteristic Auger maps or line profiles. The clusters shown here correspond to 3 different phases of a binary alloy A_xB_y. 1 : pure B ; 4 : pure A ; 2 : homogeneous phase (A_2B?). Cluster 3 signs the presence of an artefact ($C_A + C_B < 100$ %) such as a shadowing effect or the existence of a third element C and then the elements A and B are correlated in the corresponding phase. The size of a cluster gives an idea of the standard deviations and selecting a cluster it is next easy to come back to the direct space D.S. For real examples and a more precise theoretical background see refs [17, 128-130].

A clear conclusion of this subsection is that modern processing facilities permit to combine data from different sources in order to obtain more information than would be obtained from the separate processing of each image. Consequently there is the need, first, to collect the maximum of signals issued from the specimen when the incident beam is scanned.

3.6 Strategies

Between conventional quantitative AES on the one hand (sect.2) and SAM imaging on the other hand (sub. 3.5) various intermediate strategies can be developed. They depend upon the goal to be reached but the first step is obviously to obtain a good and high resolution SEM image which permits to locate the region of interest.

3.6.1 Point Analysis

If the goal is to just to identify the elements composing a small detail sits on the surface (an important application in the failure analysis of integrated circuits), it is possible to operate with a fixed probe in order to obtain a wide energy spectrum with a good signal-to-noise ratio. In this case the sensitivity is optimized by choosing a probe having the dimension of the detail. Smaller will be the probe and smaller will be the detectable details, independently from any consideration upon the relationship between the lateral resolution and the probe diameter (as discussed in subsection 3.3). The difference between two Auger spectras, one acquired on the detail and the other outside it permits easily to estimate the difference in composition between the two. Such an approach applied to polycrystalline high temperature superconductors, has indicated that most of the grain boundary surfaces were deficient in oxygen and rich in copper compared to the bulk [131]. The main risk of such an operation is that it maximizes the probability of radiation damage. Under some favourable circumstances the quantification of the detail may be performed (as it is illustrated on fig. 9 a). Consistency between the experimental spectras and the estimated compositions of the detail and of its surroundings may be verified from the use of Monte Carlo simulations. For infinitely narrow incident probe these calculations have been

widely applied to AES for estimating the signal intensities, the influence of the Auger backscattering factor and of the topographic effects [124] but also for simulating the background [39c,d, 132, 133]. They can be easily extended to probes of given shapes and sizes if their dimension is larger than 10 nm.

For smaller probes, it has to be kept in mind that most of the signal is issued from a reduced number of atoms. As it has been also indicated in subsection 3-3 this number can be deduced from the usual atomic density of solids (5.10^{22} at/cm^3) and from the volume ($\pi d_o^4 / 4\lambda \sin\theta$) from which 35-60 % -an estimate for $(1+e^{-1})$ / (1+R) - of this signal is issued. One obtains less than 100 nm^3 for this volume or around 5000 atoms for $d_o \approx 10$ nm !

This result proves the fantastic power of high resolution SAM in the detection of small amounts of matter (10^{-20} - 10^{-21} g) but it also indicates the emergence of quantum limitations for the quantification. For a fixed number of atoms, A, being irradiated by a sub 10-nm probe the detected intensity will depend upon their specific distribution in the x-y direction like it depends upon its z distribution in conventional AES (see fig. 14a for an illustration).

For larger probes the estimate of centrations is possible even when these concentrations are referred to an analyzed volume having blurred frontiers but when the atomic scale is reached the concept of concentration itself becomes questionable and the number of atoms been detected seems more appropriate for characterizing the performance of SAM instruments (see the appendix for details). As an estimate, the number of atoms being detected is less than 50 when a 1 nm probe is used [102, 103].

Another consequence from the instrumental point of view concerns the required stability for the specimen holder and for the incident probe when such fine probes are used.

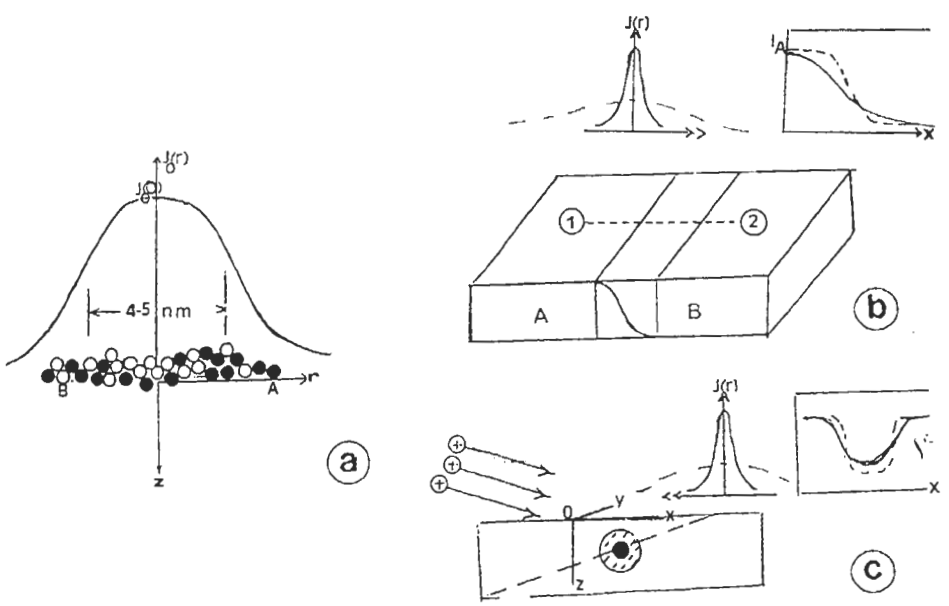

Fig. 14 a) When subten nm probes are used a significant part of the signal is issued from few hundreds of atoms. This fascinating result is paid by the fact that the characteristic signal intensity will depends upon not only the number of irradiated atoms but also upon the relative arrangement : here there is an equal number of black (A) and white (B) atoms but I(B) will be : I(B) > I(A) because of the more favourable position of the B atoms. Independently from the experimental conditions, the meaning of a concentration is questionable (for disordered systems) when the concentrations are referred to reduced volumes, V, containing a few number of atoms (because of the statistics of their respective distribution).
b)c) Strategy for analysing a concentration change along one direction $C_A(x)$, $C_B(x)$ (a grain boundary or a diffuse interface for instance) by Auger line scan technique (using probe diameters $d_o \geq 5$nm). The profile first acquired (full line) may be improved by a deconvolution technique involving the knowledge (or the simulation) of the point spread function (dashed line). b : the interface emerges from the surface ; c: the detail is buried and ion beam bevelling has to be operated before the line scan acquisition.

3.6.2 Auger Line Scan Profile

When the information of interest is only restricted to a change in composition along one direction on the surface, an Auger line scan profile parallel to this direction can be performed (for example, across a grain/grain boundary interface). In such a situation there are also some advantages to use a fine probe and a rather long dwell time for obtaining a first estimate of the concentration gradients, $C_A(x)$, $C_B(x)$, over short distances (see fig. 14 b). These estimates may be next improved from a deconvolution from the observed profile by the point Spread Function for instance (see the appendix).

The convolution effect of various PSF (given by eq. 8 and 8') by various types of sharp interfaces may be seen in ref. [96]. Of course solving the inverse problem is not easy but the scarce number of attempts in this direction is surprising with regard to the numerous attempts to solve a similar inverse problem with angle resolved XPS for non destructive in-depth profiling [74-77]. If the starting concentration values (far from the interface of interest) are accurately determined, the use of simple trying functions for $C_A(x)$, $C_B(x)$ etc (with one adjustable parameter) may certainly improve the first estimate of the concentration gradient changes with a lateral resolution of the order of the incident spot diameter. Standard deconvolution methods using Fourier transforms may also be used. For such approaches the key point is to know the radial distribution of electrons in the incident beam (instrumental effect) and to have an estimate of the radial distribution of the backscattered contribution (matrix effect). Like for the investigation of small details at fixed probe, the quantum effects have to be taken into account when sub-ten nm probes are use for obtaining an Auger line profile (see the appendix for additional details).

3.6.3 Exploring the x, y, z, Space.

Finally, it has been seen (subsections 3.2 and 3.4) that the operation of ion beam bevel sectioning (or conventional ion etching) permits to remove matter in order for an initially buried detail to become a surface detail . Such a detail (or region) of interest may be next investigated using either a fixed probe, or acquiring an Auger line scan profile or even performing elemental mapping (see fig. 14 c for a naive illustration). In principle any kind of detail located somewhere in a solid may be then analysed with a depth resolution in the nm range and a lateral resolution in the 10 nm range. One may also dream to obtain successive characteristic x, y maps acquired at different depths in order to obtain some kind of spatial mapping or characteristic Auger microtomography of a region of the specimen.

For such purposes, the present limitations are related to the acquisition time required for obtaining good Auger line scan profiles and good characteristic maps. This limitation will be partly overcome when a real parallel acquisition of the whole Auger spectrum will be possible. The other limitations are related to the physics of ion/matter interaction inducing atomic mixing and surface roughness.

Presently it remains that the exploration of the x,y,z directions is but selecting the direction(s) of interest and finding the best compromise between sensitivity and spatial spreading of the required information. In other words one may consider a hypervolume x, y, z, E_K composed of hypervoxels Δx, Δy, Δz, ΔE_K (extending the volume shown of fig .13a to a fourth dimension) and the minimum time needed for acquiring the information related to a given hypervoxel with respect to the total acquisition time : t. The strategy is defined by the goal to be reached with the optimisation of the number of hypervoxels to be selected and the amount of information contained by each of them.

4. Conclusion

The recent developments of AES concern three directions

i) The investigation of the electronic structures of surfaces from the analysis of CVV Auger lines,
ii) the improvement of quantification
iii) the improvement of the spatial resolution.

In the context of nanostructural characterization (point iii) one of most significant progress of the last years is the conquest of the third dimension (the z direction) with the combination of AES and of ion beam etching or computer controlled ion beam bevel sectionning. In the x-y directions two different priorities have been defined at Arizona State University and at York University. At ASU the goal was to minimize the incident probe size in order to optimize the detection limit (in term of minimum number of atoms detectable). Clusters composed of ~10-20 silver atoms have been then detected with an incident probe of

around 1-2 nm in diameter [102][103]. At York, the goal as to improve the quantification of SAM images by taking into account the physical processes involved in the Auger emission and detection (including the possible artefacts associated to topographic effects or the local change of the Auger backscattering coefficient). Characteristic Auger images have been acquired for applications to metallurgy, archaeology, wear and lubrication as well as to metal/semiconductor devices [17b].

The instruments presently available on the market result from a compromise between incident spot size (and intensity : few nA in 10-20 nm), and in depth profiling and elemental mapping. The use of such fine probes permits the identification of elements composing details having volumes in the 10 nm^3 range (or few hundreds of atoms). Modern processing facilities and modern methods for signal and images analysis (Multivariate Statistical Analysis and Correlation Diagrams) permits to extract the maximum of informations of the collected data.

The inherent limitations of high spatial resolution SAM are mainly related to radiation damage effects (which increase with the dose) and to topographic effects (which increase when the beam diameter is decreased).

For the future, a decisive breakthrough will be the development of a real parallel detection system for the acquisition of the whole Auger spectrum like in EELS. The collection of such a spectrum over 1024 channels (instead of 5-15 presently) will permit to combine elemental mapping and investigation of surfaces electronic structures and also to improve the quantification (with improved background substraction methods).

Similar combinations are possible in EELS and the two techniques have similar performance in term of minimum number of atoms detectable but they also have their own specificity and limitations. The specificity of SAM lies in its extreme surface sensitivity (for the investigation of the early stages of deposition, corrosion etc) associated to the recent possibility of exploring a 3d space. The dimension of the incident probe size reaching the atomic scale new formalisms have also to be developed for taking into account the effects associated to this new frontier.

Acknowledgements

For their help concerning this paper and the associated lecture the author would like to thank K. Childs (Physical Electronics, Eden Prairie) S. Hofmann (Max Planck Institute Stuttgart), O. Jbara (LASSI, University of Reims), J. Olivier and P. Etienne (Thomson CSF, Orsay) C.J. Powell (NIST Gaithersburg) M. Prutton (University of York), Dr. R. K. Champaneria (V.G. Scientific, East Grinstead), D.K. Skinner (GEC Marconi, Towcester), J.A. Venables (Arizona State Univ. and University of Sussex).

Appendix

Some concepts proposed for SAM quantification. As usual in quite all quantification procedures, one may relate the detected intensity on the specimen I(A), to that obtained on a pure element, $I^{\infty}(A)$, under the same experimental conditions.

From eq.(2) one obtains :

$$\frac{I(A)}{I^{\infty}(A)} = \int_0^{\infty} \frac{[j_o(r) + R_{A/S} j_R(r)] 2\pi r dr}{I_o(1 + R_{A/A})} \int_0^{\infty} C_A(r,z) \left[\frac{N^o}{N_A^o} \frac{e^{-z/\lambda \sin\theta}}{\lambda_A \sin\theta} \right] dz \qquad (A1)$$

where $R_{A/A}$, N_A^o and λ_A are refered to the pure standard (and then are known) while $R_{A/S}$ N^o and λ are referred to the investigated specimen and are matrix dependent. The ratio $Y_A = I(A)/I^{\infty}(A)$ is deduced in principle from measurements. The first integral can be written in the form $\int_0^{\infty} \varphi(r) 2\pi r dr$ where $\varphi(r)$ corresponds to a normalized radial distribution function. The terms into brackets of the last integral correspond to a normalized attenuation function, h(z).

Then (A_1) may also be expressed in the following form :

$$Y_A = \int_0^{\infty} \varphi(r) 2\pi r dr \int_0^{\infty} C_A(r,z) h(z) dz \qquad (A2)$$

The $\varphi(r)$ and h(z) functions are based on the same philosophy as the $\Phi(\rho z)$ and $f(\chi)$ functions (which are also matrix dependent) first suggested by Castaing [124] and now extensively used in EPMA quantification [135][136].

The product of $\varphi(r)$ by h(z) may be named the effective spatial ionization function of SAM :

$$E(r,z) = \varphi(r).h(z) \qquad (A3)$$

and it is illustrated on the top of page 2.

When the incident probe is centred on point

$M(x_o, y_o)$ the normalized Auger signal is given by :

$$Y_A(x_o, y_o) = \int_{-\infty}^{+\infty}\int_{-\infty}^{+\infty} E(x - x_o; y - y_o; z) \, C_A(x, y, z)\, dx\, dy\, dz \qquad \text{(A4)}$$

It is no more than the convolution of the E function by the spatial distribution of element A. The quantification process consists in a deconvolution of the normalized Auger profiles $Y_A(x_o,y_o)$ by the E function. Such a procedure will improve the quantification and also the localization of the species.

In practice, h(z) has to be calculated from a postulated knowledge of the depth dependence of $C_A(z)$ (such as a homogeneous distribution over 3 $\lambda \sin\theta$ or a stratified distribution) and the deconvolution procedure is restricted to the surface (x,y) in a way similar to that previously suggested [96]. For the $\varphi(r)$ function, the use of Gaussian models (see eq. 8 and 8') is possible but less naive approaches may also be followed for the description of the point spread function.

The procedure has to be repeated for all the elemental components (B,C,...) and the use of a sum rule ($\sum_{N}^{A,B,C} C_N = 100\%$) permits to verify the consistency of the results.

When subten nm probes are used, the above concepts have to be reconsidered and the discontinuous nature of atomic distributions has to be taken into account.

From the definition of the cross-section, the detected Auger intensity, i_A, related to one atom of coordinate (r_i, z_i) is [137] :

$$i_A(r_i, z_i) = [j_o(r_i) + R_{A/S} j_R(r_i)] Q_A \cdot a_{ijk} \cdot e^{-z_i/\lambda \sin\theta} \, T \qquad \text{(A5)}$$

This intensity may be normalized to the intensity of an atom A sits at the origin (0,0).

$$i_A(0,0) = [j_o(0) + R_{A/S} j_R(0)] Q_A \cdot a_{ijk} \cdot T \qquad \text{(A6)}$$

The ratio $y_A = i_A(r_i,z_i)/i_A(0,0)$ corresponds to :

$$y_A(r_i, z_i) = \frac{[j_o(r_i) + R_{A/S} j_R(r_i)] e^{-z_i/\lambda \sin\theta}}{[j_o(0) + R_{A/S} j_R(0)]} \qquad \text{(A7)}$$

and the new normalized intensity, Y'_A, correesponds to a summation over the positions of the atoms :

$$Y'_A = \sum_r \sum_z y_A(r_i, z_i) \qquad \text{(A8)}$$

From models of atomic distributions this approach permits to estimate the minimum number of atoms being detectable and it includes the Gallon's model for describing the signal attenuation [138]. Of course the developments of this appendix do not pretend to solve all the quantification problems of high lateral resolution SAM and many efforts remain to be done. Its unique goal is to attract the attention on these problems and to suggest some possible ways to follow.

References

1. P. AUGER, Compt. Rend. **177**, 169(1923) ; 180, 65 (1925) ; Compt. Rend. **182**, 773 (1926) ; Compt. Rend. **182**, 1215 (1926).
2. J.J. LANDER, Phys. Rev., **91**, 1382 (1953).
3. L.A. HARRIS, J. Appl. Phys. **39**, 1419 and 1428 (1968).
4. S. HOFMANN, Suf. Interf. Anal. **9**, 3 (1986).
5. C.J. POWELL, Le Vide, Les Couches Minces, **271**, 127 (1994).
6. T.A. CARLSON, Photoelectron and Auger electron Spectroscopy, Plenum Press N.Y. (1976).
7. D. BRIGGS and M.P. SEAH, Practical Surface Analysis, Vol. 1, 2d Ed. John Wiley and Sons Chichester (1990).
8. J.C. RIVIERE, Surface Analytical Techniques, Clarendon Press, Oxford (1990).
9. LE VIDE LES COUCHES MINCES, **271,** (Mars Avril 1994).
10. MICROSCOPY, MICROANALYSIS, MICROSTRUCTURES, Vol. **6**, n°3, 253-362, June 1995.
11. a) LE DAVIS, N.C. MAC DONALD, P.W. PALMBERG, G.E. RIACH and R.E. WEBER, Handbook of Auger Electron Spectroscopy, 2nd Ed, Physical Electronics Industries Inc, Minnesota (1976).
    b) G.E.McGUIRE, Auger Electron Spectroscopy Reference Manual, Plenum NY(1979).
    c) Y. SHIOKAWA, T. ISIDA and Y. HAYASHI, Auger Electron Spectra Catalogue - A data Collection of Elements, Anelva Corp., Tokyo (1979).
    d) T. SEKINE, Y. NAGASAWA, M. KUDOH, Y. SAKAI, A.S. PARKES, J.D.GELLER, A. MOGAMI and K.

HIRATA, Handbook of Auger Electron Spectroscopy, JEOL, Tokyo (1982).
12. J. CAZAUX, Mikrochimica Acta **Sup 12**, 37, 1992).
13. S. HOFMANN, Mikrochimica Acta, **114/115**, 21 (1994).
14. S. TANUMA, C.J. POWELL, D. R. PENN, Surf. Interface Anal. **11**, 577 (1988) ; **17**, 911 (1991) ; **17**, 927 (1991) ; **20**, 77 (1993) ; **21**, 165 (1993).
15. a) J. CAZAUX, Microsc. Microanal. Microstruct. **3**, 271 (1992)
b) C. MERLET, O. JBARA, S. RONDOT, J. CAZAUX Surf. Interface Anal. **19**, 192(1992)
16. R. SHIMIZU, Jpn, J. Appl. **22**, 1631 (1993) ; S. ICHIMURA and R.SHIMIZU, Surf. Sci. **112**, 386 (1981).
17. a) M. PRUTTON, C.G.H. WALKER, J.C. GREENWOOD, P.G. KENNY, D. BARKSHIRE, I.R. ROBERTS and M. M. EL GOMATI, Surf. Interf. Anal. : **17**, 71 (1991)
b) M. PRUTTON, in ref. 10 pp 289.
18. G.G. HEMBREE and J.A. VENABLES, Ultramicroscopy **47**, 109 (1992)
19. J. LIU, G.G. HEMBREE, G.E. SPINNLER, J.A. VENABLES, Ultramicroscopy **52**, 369 (1993).
20. J. CHAZELAS, J. CAZAUX, G. GILLMANN, J. LYNCH, R. SZYMANSKI, Surf. Interf. Anal. **12**, 45, 1988.
21. J.C. RIVIERE in ref [7] Chap. 2 p. 18 or in ref. [8] Chap. 3 p. 26.
22. J.T. GRANT, Surf. Interf. Anal. **14**, 271 (1989).
23. M.P. SEAH in Practical Surface Analysis, ref [7], p. 201, (1990).
24. C.C. CHANG in Characterization of Solid Surfaces Ed. Kane, P.F. Larrabee, G.B. Plenum Press, NY 509 (1974).
25. T.W. HAAS, J.T. GRANT and G.J. DOOLEY, J. Appl. Phys. **43**, 1853 (1972).
26. D.W. GOODMAN, R.D. KELLEY, T.E. MADEY and J.T. YATES, Jr., J. Catal. **63**, 226 (1980).
27. J.A.D. MATTHEW, M. PRUTTON, M.M. EL GOMATI and D.C. PEACOCK, Surf. Inter. Anal. **11**, 173 (1988).
28. S. TOUGAARD, Solid State Comm. 61, 547 (1987).
29. J. CHAZELAS, A. FRIEDERICH, J. CAZAUX, Surf. Interf. Anal. **11**, 36 (1988).
30. C.J. POWELL, Scanning Electron Microscopy **IV**, 1649 (1984).
31. A. JABLONSKI and C.J. POWELL, Surf. Interf. Anal. **20**, 771, (1993).
A. JABLONSKI in Springer Series in Surface Science, **18**, 186 (1989)
32. C.J. POWELL, Surf. Sci. **299/300**, 34 (1994).
33. C.J. POWELL, A. JABLONSKI, S. TANUMA, D.R. PENN, J. Electr. Spectros. Rel. Phen. 68, 605 (1994).
34. S. TANUMA, S. ICHIMURA, K. YOSHIHARA, Appl. Surf. Sci. **100-101**, 47 (1996).
35. W.H. GRIES, Surf. Interf. Anal. **24**, 38 (1996).
36. J. CAZAUX, in Surface and Interface Characterization by Electron Optical Methods, Ed. A. Howie and V. Valdre, Plenum Press, NY, NATO ASI Series B Physics, **191**, 89 (1988).
37. C.J. POWELL and M.P. SEAH, J. Vac. Sci. Technol. A. , **8**, 735 (1990).
38. C.J. POWELL and M. P. SEAH, Surf. Interf. Anal. **9**, 79 (1986).
W.A. DENCH, L.B. HAZELL, M.P. SEAH, Surf. Interf. Anal. **13**, 63 (1988).
39. a) M.P. SEAH, I.S. GILMORE, P.J. CUMPSON, J.P. LANGERON, G. LORANG, Proceedings ECASIA 96 to appear in Surf. Interf. Anal.
b) M.P. SEAH, I.S. GILMORE, J. Vac. Scien. Technol. A. **14**, 1401, (1996).
c) T. TAKEICHI, K. GOTO, V. GAIDOROVA, Appl. Surf. Sci. **100/101**, 25 (1996).
d) Z.J. DING, R. SHIMIZU, K. GOTO, Appl. Surf. Sci. **100/101**, 15, (1996).
40. T. GREBER, J. OSTERWALDER, D. NAUMOVIC, A. STUCK, S. HUFNER and L.L. SCHLAPBACH, Phys. Rev. Letters. **69**, 1947 (1992).
41. G.G. FRANK, N. BATINA, T. GOLDEN, F. LU, A.T. HUBBARD, Science **247** , 182 (1990).
42. B. AKAMATSU, P. HENOC, F. MAURICE, C. LE GRESSUS, K. RAOUDI, T. SEKINE, T. SAKAI, Surf. Interf. Anal. **15**, 7 (1990).
43. K. MARRE, H. NEDDERMAYER, A. CHASSE, P. RENNERT, Surf. Sci. **357-358**, 233 (1996).

44. M. HUANG, C.J. HARLAND, J.A. VENABLES, Surf. Intef. Anal. **20**, 666 (1993).
45. F.E. DOERN, L. KOVER, N.S. MCINTYRE, Surf. interf. Anal. **6**, 282, (1984).
46. H.E. BISHOP, Surf. Interf. Anal. **15**, 27 (1990).
P. MORIN, Surf. Sci. **164**, 127 (1985).
47. M. CINI, Sol. State Comm. **24**. 681 (1977).
48. G. SAWATZKY, Phys. Rev. Letters, **39**, 504 (1977).
49. P. WEIGHTMAN, Rep. Prog. Phys. **45**. 753 (1982).
50. D.E. RAMAKER, Crit. Revs. Sol. State and Mater. Sci. **17**, 211 (1991) : Phys. Scripta **T41**, 77 (1992).
51. P. WEIGHTMAN, H. WRIGHT, S.D. WADDINGTON, D. VAN DER MAREL, G.A. SAWATZKY, G.P. DIAKUN and D. NORMAN, Phys. Rev. B **36**, 9098 (1987).
52. P. WEIGHTMAN, Microsc. Microanal. Microstruct. **6**, 263, (1995).
53. D.E. RAMAKER, J. Electr. Spectros. Rel. Phenom. **66**, 269 (1994)
54. J. ELECTRON. SPECTROS. Rel. Phenom. **72**, 1-332 (1995).
55. P. DURUPT, M. GHAMNIA, C. JARDIN, Le Vide ; Les Couches Minces, **275**, 255 (1995).
56. S. HOFMANN, J. Electr. Spectrosc. Rel. Phen., **59**, 15 (1992).
57. J. CAZAUX and P. LEHUEDE, J. Electr. Spectros. Rel. Phen. **59** 49 (1992).
58. S. ICHIMURA, H.E. BAUER, H. SEILER, S. HOFMANN, Surf. Interf. Anal. **14**, 250 (1989).
59. A. MELCHINGER and S. HOFMANN, J. Appl. Phys. **78**, 6224 (1995).
60. J. CAZAUX, X-Ray Spectrometry **25**, 265 (1996).
61. G. OHLENDORF, W. KOCH, V. KEMPER, G. BORCHARDT, Surf. Interf. Anal. **17**, 947 (1991).
62. F. OHUCHI, M. OGINO, P.H. HOLLOWAY, G.G. PANTANO, Surf. Interf. Anal. **2**, 85 (1980).
63. J. CAZAUX, J. Appl. Phys. 59, 1418 (1986)
J. Appl. Spectrosc. Electron. **11**, 293 (1986).
64. V. GARCIA, A. GLACHANT, R. PANTEL, A. STRABONI, Appl. Surf. Sci. **74**, 165 (1994).
65. G. LORANG, J.P. LANGERON and M.P. SEAH, Proceeding ECASIA 96 to appear in Surf. Interf. Anal.
66. S. ICHIMURA and R. SHIMIZU, J. Appl. Phys. **50**, 6020, (1979).
67. C. JARDIN and D. ROBERT, Appl. Surf. Sci. **35**, 495 (1988-1989).
68. C.G. PANTANO and T.E. MADEY, Appl. Surf. Sci. 7, 115 (1981).
69. A.J.M. MENS, O.L.J. GIJZEMAN, Appl. Surf. Sci. **99**, 133, (1996).
70. J. CAZAUX, Microsc. Microanal. Microstruct. **6**, 345 (1995).
71. E. BAUER, W. TELIEPS : in Surface and Interface Characterization by Electron Optical Methods ed. by A. Howie and V. Valdré, Plenium Press, NY, **191**, 195 (1988).
72. E. BAUER in Chemistry and Physics of Solid Surfaces VIII, Springer series in Surface Sciences **22**, 267 (1991.
73. S. HOFMANN in ref. [7] p 143.
74. N. IWASAKI, R.NISHITANI, S. NAKAMURA, Jap. J. Appl. Phys. **17**, 1519 (1978).
75. M. PIJOLAT and G. HOLLINGER Surf. Sci. **105**, 114 (1981).
76. P.H. HOLLOWAY and T.D. BUSSING Surf. Interf. Anal. **18**, 251 (1992).
77. G.Y. CHERKASHININ, Surf. Sci. **74**, 67 (1995).
78. W.H. GRIES, Appl. Surf. Sci. **100/101**, 41 (1996).
79. J. CAZAUX, T. BARDOUX, D. MOUZE, J.M. PATAT, G. SALACE, X. THOMAS, J. TOTH, Surf. Interf. Anal. **19**, 197 (1992).
80. A. ZALAR, Thin Solid Films, **124**, 223 (1985).
81. S. HOFMANN in ref [7] p. 143.
S. HOFMANN Progress in Surf. Sci. **36**, 35 (1991).
82. S. HOFMANN, Appl. Surf. Sci. **70/71**, 9 (1993).
83. S. HOFMANN, Surf. Interf. Anal. **21**, 673 (1994).
84. A. ZALAR, E.W. SEIBT, P. PANJAN, Apl. Surf. Sci. 100/101, 92 (1996)
85. E.R. MALINOWSKI, D.G. HOWERY, Factor Analysis in Chemistry, Wiley NY 1980.
86. S.W. GAARENSTROOM, Appl. Surf. Sci. **7**, 7 (1981).

Appl. Surf. Sci, **26**, 561 (1986)
87. J.S. SOLOMON, Surf. Interf. ANAL. 10, 75 (1987)
88. FRESENIUS J. Anal. Ch. 353 (1995). A. JOHN p 468 ; T. WOHNER, G. ECKE, H. ROSSLER, S. HOFMANN : p 447 ; W. LISOWSKI, A.H.J. VAN DEN BERG, M. SMITHERS, V.A.C. HAANAPEL, p707.
89. T. MOROHASHI, T. HOSHI, H. NIKAIDO, M. KUDO, Appl. Surf. Sci. **100/101** 84 (1996).
90. W. BOHNE, F. FENSKE, S. KELLING, A. SCHOPKE, B. SELLE, Phys. Stat. Sol.b **194**, 69 (1996).
91. H.G.. STEFFEN, S. HOFMANN, Surf. Interf. Anal. **19**, 157 (1992).
92. C. GATTS, A. ZALAR, S. HOFMANN, M. RUHLE, Surf. Interf. Anal. **23**, 809 (1995).
93. S. HOFMANN, A. ZALAR, E.H. CIPLIN, J.J. VAJO, H.J. MATHIEU, P. PANJAN, Surf. Interf. Anal. 20, 621 (1993).
94. H.J. MATHIEU, Le Vide, **52** (279) 81 (1996).
95. P. ETIENNE, J. CHAZELAS, G. CREUZET, A. FRIEDERICH, J. MASSIES, F. NGUYEN-VAN-DAU, A. FERT, J. of Cryst. Growth, **95**, 410 (1989).
96. J. CAZAUX, Surf. Interf. Anal. **14**, 354, (1989).
97. C. MORY and C. COLLIEX, Ultramicroscopy, **38**, 330, (1989).
98. M.M. EL GOMATI and M. PRUTTON, Surf. Sci. **72**, 485 (1978).
99. J. CAZAUX, Surf. Sci. **125**, 335, (1983).
100. N.C. MAC DONALD and J.R. WALDROP, Appl. Phys. Lett. 19, 315 (1971).
101. G. TODD, H. POPPA, L. VENEKLASSEN, Thin Solid Films, 57, 213 (1979).
102. J.A. VENABLES, G.G. HEMBREE, J. LIU, C.J. HARLAND, M. HUANG, Proceed. ICEM 13, Paris, July 1994, Eds : Les Editions de Physique, **1**, 759 (1994).
103. a) J. LIU, Microbeam Analysis 1995, Proceed. 29 th MAS Conf. Breckenridge 1995, Ed. : E.S. Etz, VCH 235 (1995). b) J. VENABLES, G.G. HEMBREE, J. LIU, J.S. DRUCKER, Inst. Phys. Conf. Series, **130**, 415 (1992).
104. P. KRUIT, and J.A. VENABLES, Ultramicroscopy **25**, 183, (1988).
105. J.A. VENABLES and G.G. HEMBREE Inst. Phys. Conf. Series **119**, 33 (1991).
106. J. CAZAUX, J. CHAZELAS, M.N. CHARASSE and J.P. HIRTZ, Ultramicroscopy, **25**, 31, (1988).
107. L. FRANK, Vacuum, **42**, 147 (1991).
108. D.K. SKINNER, Surf. Interf. Anal. **14**, 567 (1989).
109. D.K. SKINNER in ref. [10] p 321.
110. M.J.G. WENHAM, I.R. BARKSHIRE, M. PRUTTON, R.H. ROBERTS and D.K. WILKINSON, Surf. Interf. Anal. **23**, 858 (1995).
111. R. WATTS, D.K. WILKINSON, I.R. BARKSHIRE, M. PRUTTON, A. CHAMBERS, Phys. Rev. B, **52**, 451, (1995).
112. I.R. BARKSHIRE and M. PRUTTON, J. Appl. Phys. **77**, 1082 (1995).
113. P.C. SCHAMBERGER, G.L. JONES, J.A. GARDELLA Jr., P.J. Mc KEOWN, L.E. DAVIS, J. Vac. Sci. Technol. A **14**, 2289 (1996).
114. O.L. KRIVANEK, C.C. AHN, R.B. KEENEY, Ultramicroscopy **22**, 103, (1987).
115. a) C. COLLIEX, Mikrochimica Acta, **114/115**, 71 (1994). b) C. COLLIEX or A. KRIVANEK or M. RUHLE, This meeting.
116. I.R. BARKSHIRE, M. PRUTTON and D.K. SKINNER, Surf. Intef. Anal. **17**, 213 (1991).
117. H. BENHAYOUNE, O. JBARA, X. THOMAS, D. MOUZE, J. CAZAUX, Surf. Interf. Anal. **20**, 600 (1993).
118. H. BENHAYOUNE, O. JBARA, X. THOMAS, J. CAZAUX, X-Ray Spectrometry, **24**, 147 (1995).
119. G. TODD, H. POPPA, J. Vac. Sci. Tech. **15**, 672 (1978).
120. M.M. EL GOMATI, J.A.D. MATTHEW and M. PRUTTON, Appl. Surf. Sci. 24, 147 (1985)
121. C.J. HARLAND and J.A. VENABLES, Ultramicroscopy, **17**, 9 (1985).
122. I.R. BARKSHIRE, M. PRUTTON, J.C. GREENWOOD and P.G. KENNY, Appl. Surf. Sci. **55**, 245 (1992).
123. a) M. CRONE, I.R. BARKSHIRE and

M. PRUTTON, Surf. Interf. Anal. 27, 857 (1994),
b) M. PRUTTON, I.R.BARKSHIRE and M.CRONE, Ultramicroscopy, **59**, 47 (1995).
c) I. R. BARKSHIRE, P.G. KENNY, W. FLETCHER, M. PRUTTON, Ultramicroscopy, **63**, 193(1996).
124. M.M. EL GOMATI, M. PRUTTON, B. LAMB, C.G. TUPPEN, Surf. interf. Anal. **11**, 251, (1988).
125. A. UMBACH, A. HOYER, R. BRUNGER, Surf. Interf. Anal. **14**, 401 (1989).
126. H. ITO, M. ITO, Y. MAGATANI, F. SOEDA, Appl. Suf. Sci. **100/101**, 152 (1996).
127. R. BROWNING, J.L. SMIALEK, N.S. JACOBSON, Adv. Ceramic. Materials **2**, 773 (1987).
128. M. PRUTTON, M.M. EL GOMATI, P.G. KENNY, J. Electr. Spectr. Rel. Phen. **52**, 197 (1990).
129. P.G. KENNY, I.F. BARKSHIRE, M. PRUTTON, Ultramicroscopy, **56**, 289 (1994).
130. I.R. BARKSHIRE, M. PRUTTON, G.C. SMITH, Appl. Surf. Sci. **84**, 331 (1995).
131. D.M. KROEGER, A. CHOUDHURY, J. BRYNESTAD, R. K. WILLIAMS, R.A. PADGETT and W.A. COGHLAN, J. Appl. Phys. **64**, 331 (1988).
132. S. ICHIMURA, Z.J. DING, R. SHIMIZU, Surf. Interf. Anal. **13**, 149 (1988).
134. Z.J. DING, T. NAGATOMI, R. SHIMIZU, K. GOTO, Surf. Sci. **336**, 397 (1995).
135. R. CASTAING, Thèse Paris 1951 and in Advances Electron. Electr. Physics **13**, 317 (1960).
136. K.F.J. HEINRICH and D.E. NEWBURY (Eds) Electron Probe Quantitation, Plenum Press NY (1991).
137. S.J.B. REED (Eds.) Electron Probe Analysis 2nd ed. Cambridge University Press (1993) Cambridge.
138. J. CAZAUX and C. COLLIEX, J. Electr. Spectro. Rel. Phen. **52**, 837 (1990).
139. T.E. GALLON, Surf. Sci. **17**, 486 (1969).